

1
2
3 On the sensitivity of computed higher tidal harmonics

4 to mesh size in a finite element model

5 by

6 J. Eric Jones and Alan M. Davies

7 Proudman Oceanographic Laboratory

8 6 Brownlow Street

9 Liverpool L3 5DA

10 England, U.K.

11 ABSTRACT

12 A finite element model of the Irish and Celtic Sea regions with a range of grid
13 resolutions is used to examine the influence of resolution upon the higher harmonics of the
14 tide in the region. Comparisons are also made with published results from finite difference
15 models of the area, and observations. Calculations using fine near-shore elements with non-
16 zero water depths in coastal regions were found to be more accurate and less time consuming
17 than those using a zero coastal water depth. A detailed examination of the spatial variability
18 of the higher harmonics in near-shore regions of the eastern Irish Sea particularly the Solway
19 and Morecambe Bay showed significant small scale variability. This together with the
20 variation in higher harmonics in the eastern Irish Sea and adjacent estuaries, clearly shows
21 the need for an unstructured grid model of the region that can include the estuaries. To
22 match the high resolution of the model in nearshore regions accurate high resolution
23 topography is required.

24 1. INTRODUCTION

25 The generation of higher harmonics of the tide by non-linear effects has been well
26 established in the literature, since the early work of Proudman in the 1960's. Numerous
27 numerical simulations of their spatial distributions in a range of shallow water regions have
28 been performed using finite difference models (e.g. for the Irish Sea region, Young et al
29 2000, Davies and Jones 1992, hereafter referenced as DJ92, Davies 1986, Davies et al. 2001,
30 Jones 1983), although to date less work has been done with finite element models. Recent
31 examples of finite element work are Fortunato et al 1997, 1999, Henich et al 2000, Legrand
32 et al (2006, 2007), Greenberg (2007) and references therein. In addition Blanton et al (2004)
33 used a finite element model to examine the principal although not the higher harmonics of
34 the tide in the South Atlantic Bight. They found that even for the principal tides it was

1 essential to have high resolution in the coastal region. Since the higher harmonics are largest
2 and show greatest spatial variability in shallow water regions then maximum resolution in
3 these areas is desirable. Consequently an unstructured grid model with enhanced resolution
4 in the coastal region would appear to be the ideal tool to simulate these harmonics. In the
5 finite difference model, the need to use a uniform grid means that the model domain is
6 generally limited in order to have a fine mesh in the coastal region without excessive
7 computational effort. A limited area coastal model therefore requires some description of
8 the higher harmonics along its open boundary which is rather restrictive. Consequently in a
9 small domain model, part of the solution has been specified through the open boundary (e.g.
10 Jones and Davies 1996, hereafter referenced as JD96, Greenberg (2007)). The alternative is
11 to use a large area model (e.g. the shelf wide model of Kwong et al 1997). In this case there
12 is no input of higher harmonics through the open boundary, since these are in deep water.
13 However, the coarse grid nature of the model means that an accurate representation of the
14 nearshore region is not possible.

15 The finite element model with its ability to vary the mesh (e.g. Henry and Walters
16 (1993), Luettich and Westerink (1995), Lynch et al (1995, 2004), Werner 1995, Malcherek
17 2000, Hervouet 2002, Jones 2002) , is able to cover a significant offshore region while
18 retaining a fine mesh near the coast. By this means a computationally efficient solution is
19 obtained. Although this means of grading the mesh, based on local water depth is popular in
20 many shallow sea models (see Greenberg (2007) for a recent review of methods in oceanic
21 and coastal situations) it is not the only approach. Recently Legrande et al (2006) developed
22 a method in which both the bathymetric field and approximate distance to offshore features
23 such as islands and reefs could be included in the mesh generation algorithm. This approach
24 was very successful in generating an optimal mesh that could resolve tidal features and re-
25 circulating eddies in regions such as the Australian Great Barrier Reef. A comparable, in the
26 sense of requiring a fine grid in the region of rapid change whilst minimizing computational
27 effort was given by Hagen et al (2002). This Local Truncation Error Analysis (LTEA)
28 approach seeks to design a mesh to make the truncation error uniform across the whole
29 domain. Recent papers (Legrande et al 2007, Greenberg 2007) present a range of parameters
30 that must be considered in the design of an optimal grid. The importance of these
31 parameters varies depending upon grid location (e.g. shelf edge, shallow sea) and processes
32 to be modelled. In the case of tidal processes Legrande et al (2007), suggest that a grid
33 aligned with the major axis of the M_2 tidal ellipse with anisotropy related to the major and
34 minor axis of the ellipse could be optimal. This approach is very attractive, although in the

1 Irish Sea example given in Legrand et al (2007) it did reduce grid resolution in near coastal
2 regions where higher harmonics are important. Although other parameters could possibly
3 also be included to enhance local resolution.

4 Despite this significant recent progress in grid design (see review of Greenberg
5 (2007)) it is clear that a major problem still remains, namely how should the grid be graded
6 from offshore to nearshore in order to obtain an accurate solution for both the fundamental
7 and higher harmonics. In a more complex region such as the west coast of Britain where
8 there are a number of channels (Fig. 1a, see Fig. 1b for details of topography in eastern Irish
9 Sea) where “wetting and drying” can occur, with associated small scale changes in the
10 higher tidal harmonics, and deep water regions adjacent to shallow (e.g. Irish Sea) the choice
11 of grid is complex. Also measurements and coarse grid shelf wide models show that the M_4
12 tide along the west coast of Britain increases from the shelf edge (where models (e.g. Davies
13 1986) assume it is zero) through the Celtic Sea with a subsequent decrease at the southern
14 end of the Irish Sea and increase in the eastern Irish Sea. This spatial distribution is very
15 different to that in a near coastal region or estuary where a uniform increase towards the
16 coast or head of the estuary occurs. The simulation of the complex M_4 distribution that
17 occurs off the west coast of Britain therefore represents a good test of the ability of an
18 irregular grid model to adequately describe the tide and its higher harmonics. Such a test is
19 performed here. In addition the existence of a solution from a high resolution finite
20 difference eastern Irish Sea model, Fig. 2 (JD96) and a comprehensive data set in terms of
21 tidal observations and bottom topography in this nearshore region, means that the sensitivity
22 to grid resolution in the coastal domain can also be examined. For this reason the area off
23 the west coast of Britain with particular emphasis on the eastern Irish Sea is used here to
24 examine the accuracy of a finite element code (TELEMAC) with a range of irregular grids,
25 to represent the fundamental constituent M_2 and its higher harmonics.

26 The primary objective of the paper is to develop an optimal irregular mesh finite
27 element model of the tides along the west coast of Britain, with particular emphasis on the
28 eastern Irish sea where a detailed (horizontal resolution of 1 km) topographic data set exists
29 (JD96). The finite element distribution will be such that it can adequately describe the
30 fundamental tide, to such an extent that the higher harmonics can be accurately reproduced.
31 Since these are largest in near coastal regions then the mesh will be refined locally,
32 particularly in the eastern Irish Sea, to allow for their correct reproduction. The focus of the
33 calculation will be the eastern Irish Sea, where the higher harmonics are significant and an

1 accurate finite difference solution and associated data (JD96) exists for comparison
2 purposes.

3 The present paper complements and extends an earlier paper (Jones and Davies 2007
4 hereafter JD07) where the focus was the influence of grid resolution upon tidal residual
5 currents. In that paper by comparison with a published finite difference solution, it was
6 shown that the removal by using finite elements of artificial vorticity associated with the
7 “staircase” representation of the coast in a finite difference model (Greenberg 2007),
8 significantly improved the representation of tidal residuals in the near coastal region. In
9 essence in a finite difference model the poor representation of the coastline corrupted the
10 tidal residual within five grid boxes of the coast. In addition JD07 examined the detailed
11 distribution and convergence of the tidal residual within the Mersey estuary for a range of
12 locally refined meshes in the estuary. Calculations showed that there were significant gyres
13 at the entrance and within the Mersey, in the tidal residual current. These gyres could only
14 be reproduced by using a finite element grid that could resolve coastal and topographic
15 variations within the Mersey. Although these convergence studies gave significant insight
16 into the role of mesh refinement, there were no tidal residual currents or elevations with
17 which comparisons could be made. Also the focus of JD07 was a convergence study within
18 the Mersey and the influence of coastal discretization method on the solution. Due to a lack
19 of observations no model data comparisons were possible.

20 In this paper the focus of the study is the influence of finite element resolution upon
21 higher harmonics of the tide that are generated by non-linear effects and “wetting and
22 drying” in the coastal region of the eastern Irish Sea. Since extensive observational data sets
23 are available over the whole region, as are published results from a finite difference model, a
24 detailed comparison with observations and comparable finite difference solutions are
25 possible. The focus here is no longer limited to the Mersey estuary as in JD07, but rather to
26 spatial variability in a range of nearshore regions where observations are available. This
27 spatial variability is illustrated in a number of figures and quantified in various tables.

28 The basic hydrodynamic equations are described in the next section. In subsequent
29 sections the influence of the nearshore coastal boundary, and finite element resolution, upon
30 the higher harmonics are considered. Conclusions as to an optimal form of the mesh and
31 sensitivity of the solution are presented in the final part of the paper.

32 2. HYDRODYNAMIC EQUATIONS

33 To examine the sensitivity of the tidal distribution to variations in horizontal grid
34 resolution, it is sufficient to solve the two dimensional vertically integrated hydrodynamic

1 equations. Since details are given in DJ92 and JD96 only the main features are presented
2 here. As the region spans a range of latitude, the hydrodynamic equations in spherical
3 coordinates were used. The model contains all the non-linear terms, including momentum
4 advection and quadratic bottom friction with a friction coefficient $k = 0.0025$, an appropriate
5 value to use in a two dimensional model and consistent with DJ92.

6 Along the open boundaries (Fig. 1a) the M_2 tidal elevation was specified, with higher
7 harmonics set to zero. Consequently the higher harmonics were generated by the model
8 dynamics. The input was identical to that used by DJ92. In all calculations (Table 1a) the
9 same tidal input was used although the finite element grid varied (Table 1b). In the finite
10 element calculations in which the grid was refined to give enhanced resolution in near
11 coastal regions with coarser resolution offshore, the tidal input was interpolated to the new
12 open boundary nodes. Solutions were determined in all cases by integrating forward in time
13 over seven tidal cycles and harmonically analysing the final cycle to yield tidal amplitude
14 and phase for the M_2 , M_4 and M_6 constituents.

15 All solutions were generated from initial conditions of zero elevation and motion at t
16 $= 0$. At a closed boundary the normal component of velocity was set to zero. In shallow
17 regions “wetting and drying” occurred over the tidal cycles. As details of this are given in
18 Jones and Davies (2005), (hereafter referenced as JD05) they will not be presented here.
19 The approach is consistent with that used by JD96 in their finite difference model, and hence
20 a comparison with that model is valid. However the nearshore solution will be sensitive to
21 the algorithm used to represent “wetting and drying” (Balzano 1998) and the nearshore
22 element resolution (see later discussion).The horizontal gradient normal to the coast of
23 alongshore velocity was taken as zero, corresponding to perfect slip.

24 3. FINITE ELEMENT SOLUTION

25 3.1 *Choice of grid*

26 In a previous paper (JD05), the M_2 tidal distribution over the west coast of Britain
27 was computed with the finite element model using a range of meshes. Calculations (JD05)
28 showed that the optimal M_2 tidal solution was obtained using a mesh refinement based on
29 water depth such that the ratio between element size and $(gh)^{1/2}$ was constant. This condition
30 has been used by a number of authors (e.g. Henry and Walters (1993), see also references in
31 the comprehensive review of Greenberg et al (2007) for other criteria and recent work by
32 Hagan et al (2002) on the LTEA approach). Calculations with both a zero and non-zero
33 water depth at the coast were performed, with the non-zero depth yielding the most accurate
34 M_2 solution at minimum computational cost (JD05). Here we examine to what extent the

1 higher harmonics M_4 and M_6 are influenced by the use of a zero or non-zero coastal water
2 depth. Taking topography and eastern Irish Sea coastline from a 1 km model of this region
3 (Fig.2) (JD96) gave an optimal M_2 tidal solution (JD05).

4 3.2 Calculation using a non-zero coastal water depth (Calc 1)

5 In an initial calculation (Calc 1, Table 1a), the optimal grid (Grid G3AX (Fig. 3))
6 used by JD05 was applied, with linear triangular elements and an advection scheme based on
7 characteristics. Since a detailed comparison of the computed M_2 cotidal chart (not shown
8 but given in JD05) with measurements is given by JD05, only the major features will be
9 examined here with comparisons at coastal and offshore gauges together with current meters
10 that illustrate the major changes (Tables 2a,b). A more detailed comparison in the eastern
11 Irish Sea is given in Table 3a. The M_2 cotidal chart is characterized by a rapid increase in
12 tidal amplitude in the eastern Irish Sea, and in the shallow channels such as the Bristol
13 Channel. Within the North Channel the amphidromic point found in measurements (George
14 1980) and high resolution models of the region (Davies et al. 2001) has been displaced
15 slightly to the north. However as discussed in Davies et al. (2004), tides in this region are
16 sensitive to small changes in the tidal distribution to the north and south of the North
17 Channel. The amphidromic point in the western Irish Sea and the overall distribution of co-
18 amplitude and co-phase lines are in good agreement with co-tidal charts based on
19 observations (e.g. Robinson 1979) and computed distributions derived from both two
20 dimensional (Jones 1983) and three dimensional (DJ92) models.

21 A detailed comparison (Table 3a) of computed and observed M_2 tidal amplitude and
22 phase at identical points (Fig 2) in the eastern Irish Sea to those used in JD96 with their high
23 resolution (of order 1 km) eastern Irish Sea model, showed that the M_2 tidal amplitude
24 determined with grid G3AX (Table 3a) was of the order of 15 cm too high. The phase error
25 was on average about 10° too high. This is an appreciably larger error than that found in
26 JD96 but can be understood in terms of differences in open boundary input to the models. In
27 the present model the open boundary forcing was located well away from the Irish Sea (Fig.
28 1a) in regions where the tidal distribution was not well known. Consequently errors in
29 boundary forcing and tidal propagation into the Irish Sea due to a lack of detailed
30 topography appear at offshore gauges S, T, U, V within the Eastern Irish Sea. On average
31 these errors were of the order of 25 cm in elevation and -15° in phase (Table 3a). On the
32 other hand the limited area model of the eastern Irish Sea (JD96) had very small errors at
33 these offshore gauges, since the open boundary of this model was of limited extent and ran

1 north-south through the Isle of Man, where the M_2 tidal distribution was well known at
2 gauges S, T, U, V. The errors in amplitude increase as the water depth shallows giving
3 errors of order 30 cm at gauges Q, R in Liverpool Bay.

4 At some coastal gauges for example Barrow (locations Y, Z and AA) there is
5 significantly more spatial variability in amplitude in the present model (Table 3a) than found
6 in the observations and in JD96. Similarly at Morecambe and Fleetwood (locations BB, CC)
7 amplitudes on grid G3AX tend to be below observed despite the fact that in offshore regions
8 the tidal amplitude is too large. To examine the reason for this in more detail it is necessary
9 to consider tidal spatial variability in the region of these locations. This was accomplished,
10 using values at nodal points close to the observation (Table 4a), where Δ is the distance
11 between the nodal point and observation.

12 Consider initially Hilbre Island, close to the entrance to the Mersey estuary. At the
13 nearest nodal point located 1.1 km away in a water depth of 9.6 m, h_c , g_c are 321 cm and
14 309° , of order 30 cm too high and 10° error in phase. However, at an equivalent point in
15 shallower water ($h = 2.0$ m), h_c , g_c are 275 (cm) and 307° , of order 20 cm too low in
16 amplitude, although with little change in phase. At two other locations namely $\Delta = 1.3$ km
17 and 1.8 km, similar variations in amplitude occur depending upon water depth. These results
18 clearly show that at a near coastal location such as Hilbre there are significant variations in
19 tidal amplitude, of order 50 cm, over short distances comparable with the element resolution
20 of the model. In addition these variations are linked to water depth suggesting that a detailed
21 description of nearshore topography is required.

22 In coastal regions of more complex topographic variation where water depths are
23 below one metre, for example Barrow RI, the variation of tidal amplitude in locations close
24 to the observation point are more drastic. At locations in close proximity ($\Delta = 1.0$ km) to the
25 observation point, there is significant “wetting and drying” over the tidal cycle, which
26 together with bottom frictional effects, appreciably reduces tidal magnitude ($h_c = 164$ cm)
27 compared with observations ($h_o = 306$ cm) and nearby points which remain wet throughout
28 the tidal cycle ($h_c = 324$ cm). At the majority of points there is little change in phase with
29 change in Δ . At nearby locations, Barrow HP and Barrow HS the tidal amplitude shows
30 similar variations with water depth to that at Barrow RI with a major decrease where drying
31 occurs (Table 4a).

32 At Morecambe, although drying does not occur at nearby points, the tidal amplitude
33 at locations adjacent to the observation point, namely points $\Delta = 0.6$ km and $\Delta = 1.5$ km from

1 it show a variation in tidal amplitude from 298 cm to 322 cm, bracketing the observed value
2 of 308 cm. This variation is large considering that water depth only varies from 3.0 m to 3.7
3 m at these two locations. Slightly farther away, $\Delta = 2.0$ km, amplitude decreases to 271 cm,
4 although again there is little change in water depth. At a comparable point ($\Delta = 2.0$ km) in
5 shallow water where drying can occur tidal amplitude is reduced to 214 cm. It is interesting
6 that there is little phase variation with the computed value of 325° being in excellent
7 agreement with the observed 326° .

8 At Fleetwood where the three nearest locations are in shallow water and drying
9 occurs, the tidal amplitude is below the observed value while slightly farther away ($\Delta = 2.3$
10 km) in deeper water ($h = 9.6$ m) the computed value exceeds the observed. These
11 calculations clearly show significant spatial variability in computed M_2 tidal amplitude in the
12 nearshore region, over quite short distances, comparable with the finite element resolution.

13 The computed M_4 co-tidal chart (Fig. 4a), shows the M_4 tidal elevation amplitude
14 increasing over the Celtic Sea region, from an input value of zero along the open boundary
15 to a maximum of 12 cm in the southern part of the Irish Sea. A subsequent decrease in the
16 western Irish Sea with a minimum to the west of the Isle of Man is evident in Fig. 4a. This
17 increase through the Celtic Sea and subsequent decrease is found in observations (Table 2b)
18 and in shelf wide numerical models (Davies 1986, Kwong et al. 1997). A rapid increase in
19 elevation within the eastern Irish Sea as the water shallows is apparent in Fig. 4a and found
20 in observations (Table 3b). At Douglas and Ramsay (locations C and J) the model slightly
21 overpredicts the M_4 tidal amplitude (Table 3b). However this overprediction is less than that
22 found by JD96 in a high resolution model of the eastern Irish Sea. In the nearshore region
23 particularly around Barrow and Morecambe, the model shows a rapid increase in M_4 tidal
24 amplitude that is also found in the observations (Table 3b). A more gradual change occurs
25 in the Liverpool Bay region with computed values in good agreement with observations.
26 These comparisons clearly show that the irregular grid has sufficient resolution to accurately
27 represent the spatial variability of the tide in the offshore Celtic and Irish Sea regions. In
28 addition the finer grid in the coastal region of the eastern Irish Sea can reproduce the rapid
29 increase in the observed M_4 tide in this area.

30 To understand the reasons for the spatial variability of the M_4 tidal elevation in the
31 nearshore region it is useful to examine its variation at a number of coastal gauges (Table
32 4b). It is evident that at Hilbre the M_4 tidal amplitude varies from 26 cm to 35 cm within 1.3
33 km of the gauge, with an associated variation of water depth from 2.0 m to 16.2 m. Also,

1 there is a significant variation in phase from 228° to 146° , reflecting the shorter wavelength
2 of this component. This variation was not found in the M_2 tide where the wavelength was
3 much larger.

4 At Barrow RI in the region where drying occurred (h less than 1.0 m) the tidal
5 amplitude was over twice that observed, although there was good agreement in phase.
6 However, at deeper water locations, the amplitude was in good agreement with observations,
7 although not the phase (Table 4b). At Barrow HP at locations close to the gauge where
8 drying did not occur amplitude and phase were in good agreement with observations. As
9 previously when drying occurred the amplitude was overestimated. Similarly at Barrow HS,
10 amplitude agreed well with observations, although phase was underpredicted. At
11 Morecambe and Fleetwood there was significant spatial variability within 2 km of the tide
12 gauge with amplitude increasing rapidly as the water shallowed.

13 The computed M_6 co-tidal chart, shows (Fig. 4b) a rapid increase in tidal amplitude
14 in shallow water regions due to an increase in bottom friction. In the eastern Irish Sea there
15 is a gradual increase in the Liverpool Bay region as the water shallows. However, farther
16 north off the coast of Cumbria the M_6 tidal amplitude rapidly increases as the coast is
17 approached. These spatial changes in M_6 reflect the spatial variability in the bottom
18 topography in these regions (Fig. 1b). The spatial variability of computed M_6 tidal elevation
19 amplitude in the eastern Irish Sea is also found in the observations (Table 3c).

20 It is evident from Table 3c, that at a number of shallow water locations the model
21 tends to overpredict the value of the M_6 tidal elevation amplitude. To understand the reason
22 for this it is useful to examine its spatial variability (Table 4c). As found previously for the
23 M_4 component at Hilbre, the M_6 tidal amplitude increases rapidly as the water shallows
24 giving rise to a major overprediction of amplitude, although a reasonable phase value. In
25 deeper water the amplitude is still overpredicted with a large phase error. However, at
26 Barrow RI in drying regions, the amplitude is only slightly overpredicted, whereas in deeper
27 water the error increases, with a rapid change in phase over distances of the order of 1 km.
28 Similar rapid changes in phase occur at Barrow HP, again with amplitude decreasing in
29 shallow water. At Barrow HS the water depth in the region of the gauge varies from 5.4 m
30 to 8.0 m with no drying area. Consequently amplitude and phase change gradually over the
31 region (Table 4c).

1 At Morecambe and Fleetwood the M_6 tidal amplitude is overpredicted at all locations
2 in the region of the gauge. Also, the phase changes rapidly over short distances. This
3 suggests that the spatial variability of the M_6 tide is under-resolved in the model.

4 The computed M_2 tidal ellipse distribution over the whole region (not presented)
5 shows near circular ellipses at the southern end of the Celtic Sea, changing to a rectilinear
6 flow aligned with the coastline in St. George's Channel. Away from the coastal boundary, at
7 the entrance to the Bristol Channel there is a region of near circular current ellipses. A
8 rectilinear flow aligned with the channel axis is evident in the North Channel. Within the
9 central Irish Sea to the west of the Isle of Man, a region of near zero tidal currents is
10 apparent. This distribution of tidal currents is in good agreement with measurements (Table
11 5a, also see JD05) and results from a uniform grid finite difference model of the west coast
12 of Britain (DJ92). Although the tidal currents in the region exhibit some vertical variation,
13 this is primarily due to frictional effects in the near bed region (JD96). Consequently
14 currents above this region (i.e. those in Tables 5a-c and 6) are not appreciably different from
15 the depth mean derived by averaging observed current in the vertical. The M_2 tidal current
16 ellipses within the eastern Irish Sea are aligned in a west-east direction, with an area of
17 reduced current strength to the east of the Isle of Man (Fig. 5a(i)). The distribution of M_2
18 current ellipses in the eastern Irish Sea is in good agreement with a limited area high
19 resolution finite difference model of the region given by JD96 and observations (Table 5a).
20 The enhanced mesh resolution that can be achieved with the finite element model in the
21 eastern Irish Sea is evident in the distribution of current ellipses in the expanded plot of this
22 region shown in Fig. 5a(i). The enhanced resolution in the nearshore and estuarine regions
23 (Fig. 5a(ii)) which is possible with the finite element mesh gives significantly more detail
24 than that presented in JD96. For example in the Solway (Fig. 5a(i)) the rapid decrease in
25 current magnitude and change of orientation of the ellipse is resolved significantly better
26 than in JD96. Similarly the higher resolution in Morecambe Bay enables the spatial
27 variability in magnitude and orientation of the M_2 current ellipses to be resolved to a greater
28 accuracy than in JD96. A significant improvement in resolution in the Liverpool Bay region
29 (Fig. 5a(ii)) above that used by JD96, enables the rapid increase in magnitude and orientation
30 of tidal currents in the Mersey entrance to be resolved in the model. In JD96 the Liverpool
31 Bay region was significantly under-resolved even with a 1 km horizontal grid. In terms of
32 recent measurements at a coastal observatory in the region (Proctor and Howarth 2003) high
33 accuracy in this region is essential to understand the dynamic interactions between Liverpool
34 Bay and the Mersey River.

1 The spatial distribution of the major and minor axis of the M_4 tidal current ellipse
2 over the whole region (not presented) shows that in deep water regions these tidal currents
3 are small. However, in coastal regions particularly in the vicinity of headlands, the non-
4 linear advective terms lead to a significant generation of M_4 currents. The rapid increase in
5 M_4 tidal current magnitude and enhanced spatial variability in the near coastal region of the
6 eastern Irish Sea is clearly evident in Fig. 5b(i). This spatial variability in amplitude of M_4
7 tidal currents and ellipse orientation is comparable to that found by JD96 in the region and in
8 good agreement with observations (Table 5b). Since the M_4 generation is primarily in the
9 nearshore and estuarine regions then the enhanced resolution which is possible in these areas
10 with the finite element grid is more important for M_4 than M_2 .

11 An expanded plot of the Solway region (not presented) clearly shows an increase in
12 M_4 currents in the region where the orientation of the estuary changes from north-south to
13 west-east. In this area the M_2 tidal currents are strong and there is a rapid change in their
14 orientation which through the non-linear momentum advection term leads to a local
15 maximum in the M_4 ellipse. To the south of this region and near the head of the estuary
16 where M_2 tidal currents are weaker and do not change direction, the M_4 tidal currents are
17 reduced.

18 In Morecambe Bay it is evident (Fig. 5a(i)) that the M_2 tidal currents increase
19 towards the head of the Bay, and then rapidly decrease due to bottom friction in the shallow
20 near coastal regions at the top of the bay. Associated with this variation in tidal current
21 magnitude is a change in orientation of the current ellipse, which gives rise to the M_4 current
22 distribution shown in Fig. 5b(i). The level of detail presented here is a significant
23 improvement on that given in JD96. Similarly in Liverpool Bay (Fig. 5b(ii)), the enhanced
24 resolution in the near coast region which is present in the finite element mesh enables the
25 near coastal generation of the M_4 tide to be accurately resolved, whereas in JD96, the
26 Liverpool Bay region adjacent to the Mersey River was barely resolved.

27 The spatial distribution of M_6 current ellipses over the whole domain (not presented)
28 clearly shows that these currents are negligible in deep water offshore regions, and only
29 become important close to the coast. The plot of M_6 tidal currents in the eastern Irish Sea
30 shows (Fig. 5c(i)) significant spatial variability in current magnitude and orientation in this
31 region comparable to that found by JD96, and in reasonable agreement with observations in
32 the region (Table 5c). The higher resolution made possible by the use of a finer mesh
33 (compared to JD96) in the near coastal region allows nearshore details to be resolved to a
34 greater degree than previously. The significant improvement compared to JD96 in nearshore

1 resolution resulting from using the finite element mesh is clearly evident in the Solway
2 estuary and Morecambe Bay (Fig. 5c(i)). This figure shows that as for the M_4 tide, the M_6
3 tidal current is also a maximum in shallow water. However, the region of maximum M_6 tidal
4 currents does not correspond to that found for the M_4 tide. This is because bottom frictional
5 effects are a major source of the M_6 component of the tide, rather than the non-linear
6 momentum term. Consequently the M_6 tidal current increases as water depth decreases and
7 M_2 tidal velocity increases giving rise to enhanced bottom friction. This explains the
8 increase in M_6 currents as water depth decreases, with a subsequent decrease as M_2 tidal
9 currents are reduced in very shallow water. Although the calculations of JD96 indicated this
10 behaviour they could not resolve M_6 tidal currents to the level of detail shown in Figs. 5c(i).
11 Similarly in the Liverpool Bay/Mersey region the rapid increase in M_6 tidal currents at the
12 mouth of the river Mersey (Fig. 5c(ii)) could not be resolved by JD96.

13 It is apparent from Table 5a (Calc 1), that at some locations, for example Rig Nos.
14 15, 16 and 23, the computed M_2 tidal current amplitude is significantly overestimated. The
15 reason for this can be understood in terms of the significant spatial variability of M_2 currents
16 in the vicinity of these observations (Table 6). For example at Rig 15, A_c changes from 44
17 cm s^{-1} to 30 cm s^{-1} (in essence bracketing the observed value of 37 cm s^{-1}) as Δ varies from
18 2.2 km to 4.0 km (Table 6). Similarly at Rig 16, as Δ increases from 1.0 km to 3.7 km, A_c
19 decreases from 40 cm s^{-1} to 37 cm s^{-1} (a value in good agreement with observations). A
20 significantly larger change occurs at Rig 23, with A_c decreasing from 68 cm s^{-1} to 41 cm s^{-1}
21 as Δ changes from 0.9 km to 2.6 km.

22 The computed M_4 tidal currents are appreciable (exceed 10 cm s^{-1}) at locations 18, 24
23 and 32 (Table 5b). A similar increase in M_4 tidal currents in these regions was found in
24 JD96. This suggests that despite differences in grid size and approach (finite element,
25 compared with finite difference JD96) the offshore variability of M_4 tidal currents is being
26 reproduced in both finite element and finite difference models. To examine to what extent
27 local spatial variability influences the M_4 tidal current amplitude, both a deep water (location
28 6) and a nearshore (location 18) point are examined (Table 6). It is evident that at Posn. 6, in
29 deep water ($h = 53$ m) there is only limited spatial variability in the magnitude (A_c) and
30 orientation (T_c) of the semi-major axis. However, at Posn. 18 in shallow water $h_o = 3$ m, A_c
31 varies from 25.2 cm s^{-1} to 11.8 cm s^{-1} bracketing the observed value of 21.9 cm s^{-1} , with T_c
32 varying from 56° to 100° ($T_o = 64^\circ$). As with the elevation comparisons this suggests a lack
33 of resolution in the near coastal region.

1 The M_6 tidal currents (Table 5c) are on average small (of order 3 cm s^{-1}). The local
2 intensification at positions 24 and 32 was also found by JD96 and DJ92. On average values
3 given in Table 5c were larger than those found by JD96 and more comparable to the M_2
4 calculation of DJ92. As pointed out in JD96 the use of a larger set of tidal constituents,
5 namely M_2 , S_2 , N_2 , K_1 , O_1 as in JD96 and DJ92 tended to reduce the M_6 current magnitude
6 and probably explains its overprediction in the present calculation.

7 A detailed study (Table 6) of the spatial variability of M_6 currents in the Morecambe
8 Bay region from deeper water (Posn. 23, $h_o = 20 \text{ m}$) (Fig. 1b) to nearshore Posns. 24 and 32,
9 showed significant spatial variability in the nearshore region for example at Posn. 24 as Δ
10 changed from 1.3 km to 1.5 km, A_c decreased from 9.1 cm s^{-1} to 3.6 cm s^{-1} , although the
11 ellipse orientation T_c and water depth varied very little. Similarly at Posn. 32, as Δ changed
12 from 1.6 km to 1.7 km, A_c increased from 3.5 cm s^{-1} to 14.2 cm s^{-1} with T_c varying from 59°
13 to 122° , associated with a reduction in water depth from 11 m to 5 m. This again suggests
14 rapid spatial variability in the nearshore region with associated implications for model
15 element resolution and the need for detailed topography. Results from this calculation
16 clearly show the importance of high resolution in the near coastal regions in order to
17 accurately resolve the higher harmonics of the tide.

18 3.3. *Calculation using a zero coastal water depth (Calc 2, Grid G3A)*

19 In a subsequent calculation (Calc 2, Table 1a) the same criterion used for mesh
20 generation as in Calc 1 was applied. However, in order to generate a fine nearshore grid (Fig
21 6, Grid G3A) a zero water depth condition was applied at the coast. As shown by JD05 this
22 approach lead to a less accurate M_2 tidal solution than previously, and a significantly longer
23 run time than in Calc 1 (Table 1b) due to increased “wetting and drying” occurring in the
24 coastal region. Although the overall solution was less accurate, in offshore regions the M_2
25 tide was not substantially different to that found in Calc 1. Major differences that occurred
26 were principally confined to the near coastal regions, in particular in the eastern Irish Sea
27 and to higher harmonics of the tide. Consequently in order to determine differences in the
28 higher harmonics between Calcs 1 and 2 we will concentrate on the eastern Irish Sea. This
29 region has the added advantage that a high resolution finite difference solution already exists
30 (JD96) with associated observations that can be used in the comparisons. In addition an
31 optimal graded mesh is required in this region to complement a coastal observatory.

32 It is evident from Table 3a, that M_2 tidal amplitudes computed with grid G3A (Calc
33 2) are on average lower than those derived with grid G3AX (Calc 1) reflecting increased

1 energy loss in the shallow water regions that are resolved on this grid. This not only affects
2 coastal gauges, but offshore locations Q, R, S, T, U, V within the eastern Irish Sea.
3 Although the amplitude changes significantly, there is a minor phase change, of order one or
4 two degrees (Table 3a).

5 As in Calc 1, there is an appreciable change in amplitude, although not phase of the
6 M_2 tide in shallow water locations such as Hilbre, Barrow, Morecambe and Fleetwood
7 associated with small changes in Δ (Table 4a). Since grid G3A resolves the near coastal
8 region, at a number of locations water depths are below 1 m, and extensive “wetting and
9 drying” occurs with an associated decrease in tidal amplitude (Table 4a).

10 At offshore locations Q, R, S, T, U, V the M_4 tidal amplitude is reduced slightly from
11 that found previously, with a 10° reduction in phase (compare Calcs 1 and 2) in Table 3b.
12 For tidal amplitude this improves the agreement with observations, particularly at Q and R,
13 although not the phase. At coastal locations the M_4 tidal amplitude is in general significantly
14 overpredicted as a result of “wetting and drying” occurring at the nearest nodal point to the
15 gauge due to the increased resolution in the nearshore region. The effect of “wetting and
16 drying” upon M_4 tidal amplitude, and how this influences spatial variability is clearly evident
17 in Table 4b. For example at Hilbre, M_4 amplitude changes from 17 cm to 22 cm as Δ
18 increases from 0.6 km to 1.0 km, bracketing the observed value of 20 cm. With $\Delta = 1.2$ km,
19 water depth drops below 1 m, and “wetting and drying” occurs with an associated increase in
20 amplitude to 66 cm (Table 4b). Similarly at Barrow RI, HP and HS in shallow wet/dry
21 regions M_4 amplitude exceeds 60 cm, whereas in water depths of order 10 m, its value is
22 about 14 cm. This value is considerably lower than the observed and computed (Calc 1)
23 values of order 30 cm (28 cm computed) (Barrow RI) and 26 cm (28 cm computed) (Barrow
24 HP) found in Calc 1 in comparable water depths. This suggests, as found for the M_2 tide,
25 that the inclusion of extensive wetting/drying regions has removed significant tidal energy.
26 A similar picture emerges at Morecambe and Fleetwood with large M_4 tidal amplitudes in
27 wet/dry regions and underpredicted values in deeper water. As previously (Calc 1) in non-
28 wet/dry regions the M_6 amplitude is larger than observed (Table 3c) with on average a
29 significant reduction in areas where drying occurs. The effect of the finer grid is to
30 introduce appreciably larger spatial variability over shorter distances than found in Calc 1
31 (Table 4c).

32 The “wetting/drying” algorithm used here has been specifically chosen to be
33 consistent with that used by JD96 in their finite element calculations. However a range of

1 methods exists in the literature (see the review of Balzano 1998). Naturally different
2 approaches combined with different methods of choosing mesh refinement in near coastal
3 regions will affect the solution in these regions. Such a detailed study is however outside the
4 scope of this paper.

5 The main features of the distribution of M_2 tidal current ellipses in the eastern Irish
6 Sea (not shown) are comparable to those found previously (Fig. 5a(i)). However, it is
7 evident that in the near coastal region the use of a zero water depth condition gives rise to
8 increased resolution close to the coast. In this region the water is shallow, and the resulting
9 increase in bottom friction leads to a reduced M_2 tidal current at nodes adjacent to a coastal
10 boundary (not shown). This effect could be clearly seen in a comparison of expanded plots
11 of the Solway Firth, Morecambe Bay (not presented) and Liverpool Bay/Mersey River (Fig.
12 7a) compared with M_2 tidal ellipses computed with Grid G3AX. However, away from the
13 nearshore region there were no substantial differences in the M_2 tidal currents, as is evident
14 from Table 4a.

15 Similarly for the M_4 component of the tide, differences between solutions using
16 Grids G3AX and G3A (Calcs 1 and 2) were only evident in near coastal regions. From a
17 comparison of solutions in the Solway (not shown) and Morecambe Bay (not shown) it is
18 evident that in near coastal areas M_4 tidal currents computed with grid G3AX (non-zero
19 water depth at the coast) were slightly larger than those computed with grid G3A (zero water
20 depth at the coast). This arises because in G3A, the nearshore M_2 tidal current has been
21 reduced and hence the generation of an M_4 current is also reduced.

22 This effect is clearly evident in the Liverpool Bay region, where the nearshore M_4
23 current ellipses computed with mesh G3A (Fig. 7b) in the near coastal region (e.g. along the
24 Welsh coast to the west of the Dee estuary) are appreciably smaller than those computed
25 with mesh G3AX (Fig. 5b(ii)). Also slightly farther offshore (e.g. at 53.4° , -3.35°W) there
26 are some differences in current magnitudes and ellipse orientation. This suggests that for the
27 M_4 tide the influence of coastal water depth is not just confined to nodal points in the
28 nearshore region, but does spread some way offshore.

29 As previously the M_6 tidal current is mainly affected by differences in the G3AX and
30 G3A mesh in the near coast region. This is clearly evident in the upper reaches of the
31 Solway (not shown) where the region of M_6 currents exceeding 25 cm s^{-1} has been reduced
32 compared to that computed with grid G3AX, due to a decrease in M_2 tidal currents through
33 friction effects. However farther south in a deeper central channel at about 54.9°N , -3.5°W ,

1 and in the deeper water regions to the south of this, there is a slight increase in M_6 current
2 between grid G3A and G3AX. The reason for this is not obvious, but is in part related to the
3 fact that changes in grid representation in the neashore region as in the M_4 case do influence
4 nodal solutions farther offshore.

5 The increase in M_6 currents within the Moricambe Bay (approximate location
6 54.9°N , -3.3°W) region of the Solway (not shown) compared to that computed with grid
7 G3AX, reflects the increase in “wetting and drying” in this region due to the shallower near
8 coast water depths in G3A compared to G3AX. The harmonic analysis of a time series in
9 which “step like transitions” have occurred due to “wetting and drying” gives rise to a
10 “Gibbs type” phenomenon (Hall and Davies 2004) which leads to an increase in amplitude
11 of the higher harmonics.

12 Differences in M_6 tidal currents are also evident in Morecambe Bay (not shown),
13 particularly in the shallow northern part where the reduction in near coastal water depths in
14 grid G3A, leads to a reduction in M_6 tidal currents compared to G3AX. However, as in the
15 Solway, in some shallow embayments (e.g. at location -54°N , -2.9°W), M_6 currents
16 computed with grid G3A are larger than G3AX due to wetting and drying.

17 Differences in the near coastal and adjacent offshore M_6 currents in the Liverpool
18 Bay region between grids G3A and G3AX are evident from a comparison between Figs 7c
19 and 5c(ii). This is consistent with the differences in the M_4 solutions and confirms that the
20 influence of changes in representing coastal water depths affects the nearshore distribution of
21 the higher harmonics.

22 The influence of differences in grid G3A compared with grid G3AX upon spatial
23 variability of M_2 currents in the region of offshore current meters (Table 6) for example Rigs
24 15 and 16, is small, and less than the differences found between nearest nodes, namely
25 within the model’s resolution. At shallower near coastal locations, for example Rig 23,
26 (Table 6) at the nearest point to the observation ($\Delta = 0.7$ km) the computed value using G3A
27 is in good agreement with the observed and significantly more accurate than found with
28 G3AX. Similarly at $\Delta = 2.5$ km the magnitude although not the orientation is in better
29 agreement on grid G3A than G3AX. This suggests that for the M_2 tidal currents the
30 enhanced resolution in the near coastal region due to using G3A improves the solution.

31 For the M_4 tidal current in deeper water, namely location 6 (Table 6), the improved
32 grid resolution using G3A leads to enhanced accuracy. In shallow regions namely Rig 18

1 the solution shows similar spatial variability to that found with grid G3AX, suggesting that
2 the grid is still not sufficiently fine to resolve small scale variations in M_4 tidal currents.

3 For M_6 , as for the elevation, the current amplitude is on average significantly higher
4 than observed (Table 6) and shows appreciable nearshore variability as indicated at current
5 meters at the entrance to Morecambe Bay (Rig 23) and within the Bay (Rigs 24 and 32).
6 The spatial variability in this region using grid G3A is comparable to that using G3AX and
7 suggests that neither has sufficient resolution to represent the small scale variability of M_6 in
8 this region.

9 4. CONCLUDING REMARKS

10 A west coast unstructured grid model covering the same region as the finite
11 difference model of DJ92 with enhanced resolution in the eastern Irish Sea, comparable to
12 that of JD96, has been used to examine the sensitivity of the M_2 , M_4 and M_6 tides to
13 variations in the finite element mesh. Comparisons with observational data particularly in
14 the eastern Irish Sea and with results from JD96 using a uniform mesh eastern Irish Sea
15 model have been made.

16 Initial results using grid G3AX in which the nearshore water depth was taken as non-
17 zero, showed that an accurate distribution of the M_2 , M_4 , and M_6 tide could be obtained
18 throughout the region. By refining the mesh within the eastern Irish Sea, a solution
19 comparable to the limited area high resolution model of JD96 could be obtained even though
20 a coarse mesh was used outside this region in deeper water. Despite the coarser nature of the
21 mesh in the deeper Celtic Sea region the model could reproduce the observed spatial
22 variability of the tide in this region.

23 Calculations using grid G3A, where water depths were zero at the coast, showed that
24 in deeper water the tide changed very little, although in coastal regions there were some
25 slight modifications particularly to the distribution of the higher harmonics. However as
26 shown by JD05 on average for the M_2 tide the solution was not as accurate as using grid
27 G3AX and the computational effort was significantly larger. For this reason a non-zero
28 coastal water depth was the optimum choice when computing the fundamental and higher
29 harmonics. The calculations presented here using grid G3AX are presently being extended
30 to the simulation of storm surges and comparison with corresponding finite difference
31 solutions. Results of this intercomparison will be reported in due course.

32 33 ACKNOWLEDGEMENTS

1 The origin of the TELEMAC SYSTEM is EDF-LNHE and is therefore © EDF-
2 LNHE. Thanks are also due to Mrs L. Parry for typing the paper.
3

1 **References**

- 2 Balzano, A. (1998) Evaluation of methods for numerical simulation of wetting and drying in
3 shallow water flow models. *Coastal Engineering*, 34, 83-107.
- 4 Blanton, B., Werner, F., Seim, H., Luettich Jr., R., Lynch, D., Smith K., Voulgaris, G.,
5 Bingham, F. and Way, F. (2004) Barotropic tides in the South Atlantic Bight.
6 *Journal of Geophysical Research*, 109 (C12), C12024.
- 7 Davies, A.M. (1986) A three-dimensional model of the northwest European continental
8 shelf with application to the M₄ tide. *Journal of Physical Oceanography*, 16, 797-
9 813.
- 10 Davies, A.M. and Jones, J.E. (1992) A three dimensional model of the M₂, S₂, N₂, K₁ and
11 O₁ tides in the Celtic and Irish Sea. *Progress in Oceanography*, 29, 197-234.
- 12 Davies, A.M., Hall, P., Howarth, M.J., Knight, P and Player, R. (2001) Comparison of
13 observed (HF Radar and ADCP measurements) and computed tides in the North
14 Channel of the Irish Sea, *Journal of Physical Oceanography*, 31, 1764-1785.
- 15 Davies, A.M., Hall, P., Howarth, M.J., Knight, P and Player, R. (2004) Tidal currents,
16 energy flux and bottom boundary layer thickness in the Clyde Sea and North Channel
17 of the Irish Sea. *Ocean Dynamics*, 54, 108-125.
- 18 Fortunato, A.B., Baptista, A.M. and Luettich, R.A. (1997) A three-dimensional model of
19 tidal currents in the mouth of the Tagus estuary. *Continental Shelf Research*, 17,
20 1689-1714.
- 21 Fortunato, A.B., Oliviera, A. and Baptists, A.M. (1999) On the effect of tidal flats on the
22 hydrodynamics of the Tagus estuary. *Oceanologica Acta*, 22, 31-44.
- 23 George, K.J. (1980) Anatomy of an amphidrome. *Hydrographic Journal*, 18, 5-12.
- 24 Greenberg, D.A., Dupont, F., Lyard, F.H., Lynch, D.R. and Werner, F.E. (2007) Resolution
25 issues in numerical models of oceanic and coastal circulation. *Continental Shelf*
26 *Research* (in press).
- 27 Hall, P. and Davies, A.M. (2005) The influence of sampling frequency, non-linear
28 interaction, and friction effects upon the accuracy of the harmonic analysis of tidal
29 simulations. *Applied Mathematical Modelling*, 29, 533-552.
- 30 Hagen, S., Westerink, J., Kolar, R., Horstmann, O. (2001) Two dimensional unstructured
31 mesh generation for tidal models. *International Journal for Numerical Methods in*
32 *Fluids*, 35, 669-686.

- 1 Hagen, S.C., Horstmann, O., Bennett, R.J. (2002) An unstructured mesh generation
2 algorithm for shallow water modeling. *International Journal of Computational Fluid*
3 *Dynamics*, 16(2), 83-91.
- 4 Heniche, M., Secretin, Y., Boudreau, P. and Leclerc, M. (2000) A two-dimensional finite
5 element drying-wetting shallow water model for rivers and estuaries. *Advances in*
6 *Water Resources*, 23, 359-372.
- 7 Henry, R. and Walters, R. (1993) Geometrically based, automatic generator for irregular
8 networks. *Communications in Numerical Methods in Engineering*, 9, 555-566.
- 9 Hervouet, J-M (2002) TELEMAC modelling system: an overview. *Hydrological Processes*,
10 14, 2209-2210.
- 11 Jones, J.E. (1983) Charts of the O_1 , K_1 , N_2 , M_2 and S_2 tides in the Celtic Sea including M_2
12 and S_2 tidal currents. Institute of Oceanographic Sciences, Report No. 169, 55pp.
- 13 Jones, J E and Davies, A M (1996) A high resolution three dimensional model of the M_2 ,
14 M_4 , M_6 , S_2 , N_2 , K_1 , and O_1 tides in the eastern Irish Sea. *Estuarine Coastal and Shelf*
15 *Science* 42, 311-346.
- 16 Jones, J.E. (2002) Coastal and shelf-sea modelling in the European context. *Oceanography*
17 *and Marine Biology: an Annual Review*, 40, 37-141.
- 18 Jones, J.E. and Davies, A.M. (2005) An intercomparison between finite difference and finite
19 element (TELEMAC) approaches to modelling west coast of Britain tides. *Ocean*
20 *Dynamics*, 55, 178-198.
- 21 Jones, J.E. and Davies, A.M. (2007) On the sensitivity of tidal residuals off the west coast of
22 Britain to mesh resolution. *Continental Shelf Research*, 27, 64-81.
- 23 Kwong, C.M., Davies, A.M. and Flather, R.A. (1997) A three dimensional model of the
24 principal tides on the European Shelf. *Progress in Oceanography*, 39, 205-262.
- 25 Legrand, S. Deleersnijder, E., Hanert, E., Legat, V. and Wolanski, E. (2006) High-
26 resolution, unstructured meshes for hydrodynamic models of the Great Barrier Reef,
27 Australia. *Estuarine, Coastal and Shelf Science*, 68, 36-46.
- 28 Legrand, S. Deleersnijder, E., Delhez, E. and Legat, V. (2007) Unstructured, anisotropic
29 mesh generation for the Northwestern European continental shelf, the continental
30 slope and the neighbouring ocean. *Continental Shelf Research* (in press).
- 31 Luettich, R., Westerink, J. (1995) Continental shelf scale convergence studies with a
32 barotropic tidal model. In: Lynch, D.R., Davies, A.M. (Eds.), *Quantitative Skill*
33 *Assessment for Coastal Ocean Models*. *Coastal and Estuarine Series*, 47, American
34 Geophysical Union, Washington, DC, pp. 349-371.

- 1 Lynch, D., Ip. J., Naimie, C., Werner, F. (1995) Convergence studies of tidally-rectified
2 circulation on Georges Bank. In: Lynch, D., Davies, A. (Eds.), Quantitative Skill
3 Assessment for Coastal Ocean Models. Vol. 47, American Geophysical Union, pp.
4 153-174.
- 5 Lynch, D.R., Smith, K.W., Blanton, B.O., Luettich, R.A., Werner, F.E. (2004). Forecasting
6 the coastal ocean: Resolution, tide and operational data in the South Atlantic Bight.
7 Journal of Oceanic and Atmospheric Technology, 21(7), 1074-1085.
- 8 Malcherek, A. (2000) Application of TELEMAC-2D in a narrow estuarine tributary.
9 Hydrological Processes, 14, 2293-2300.
- 10 Proctor, R. and Howarth, M.J. (2003) The POL Coastal Observatory. In 'Building the
11 European Capacity in Operational Oceanography', Proc. 3rd International
12 Conference on EuroGOOS, 3-6 December 2002, Athens, Greece. Elsevier
13 Oceanography Series, 69: 548-553. 698pp.
- 14 Robinson, I.S. (1979) The tidal dynamics of the Irish and Celtic Seas. Geophysical Journal
15 of the Royal Astronomical Society, 56, 159-197.
- 16 Werner, F.E. (1995) A field test case for tidally forced flows: a review of the tidal flow
17 forum pg. 269-284 in Quantitative Skill Assessment for Coastal Ocean Models, ed.
18 D.R. Lynch and A.M. Davies, published American Geophysical Union.
- 19 Young, E.F., Aldridge, J.N. and Brown, J. (2000) Development and validation of a three-
20 dimensional curvilinear model for the study of fluxes through the North Channel of
21 the Irish Sea. Continental Shelf Research, 20, 997-1035.

22
23
24

1 Captions for Figures

- 2 Fig. 1: (a) Topography and place names over the whole region, (b) expanded plot of
3 topography in eastern Irish Sea and local place names.
- 4 Fig. 2: Locations of eastern Irish Sea gauges (with sample of finite difference grid of
5 JD96) used in the comparisons.
- 6 Fig. 3: Finite element Grid 1 (G3AX) used in Calc. 1.
- 7 Fig. 4: Computed (Calc. 1, Grid G3AX) (a) M_4 (i) whole region, (ii) Eastern Irish Sea,
8 (b) M_6 (i) whole region, (ii) Eastern Irish Sea, interpolated from nodal values,
9 with co-amplitude lines in cms.
- 10 Fig 5: Distribution of the major and minor axis of (a) M_2 , (b) M_4 , (c) M_6 current ellipse
11 for (i) the eastern Irish Sea, (ii) Liverpool Bay (Calc. 1, Grid G3AX).
- 12 Fig. 6: Finite element Grid G3A (zero water depth at the coast) as used in Calc. 2.
- 13 Fig. 7: Distribution of major and minor axis of (a) M_2 , (b) M_4 , (c) M_6 current ellipse in
14 Liverpool Bay, derived from Calc 2 (Grid G3A).

15
16
17
18
19

1 Table 1a: Summary of Calculations

Calc	Nature of Grid
1	Grid G3AX, element size determined by $(gh)^{1/2}$, with non-zero water depth at coast.
2	As Calc 1, but element size determined by $(gh)^{1/2}$, with zero water depth at coast. Grid G3A.

2

3

4 Table 1b: Summary of grid, nodes, run times and main features of each calculation

Calc	Grid	Nodes	Run time	Notes
1	G3AX	6842	1h 36m	h non-zero at coast.
2	G3A	11702	10h 02m	h zero at coast.

5

6

1 Table 2a: Latitude and longitude of tide gauges used in comparison tables

Point	Port	Latitude (N)	Longitude(W)
Eastern Irish Sea:			
A	Barrow	54.0944	3.2236
B	Birkenhead	53.4000	3.0167
C	Douglas	54.1461	4.4667
D	Heysham	54.0333	2.9167
E	Hilbre	53.3833	3.2167
F	Liverpool	53.4083	2.9983
G	Formby	53.5667	3.1167
H	Hestan	54.8333	3.8000
I	Liverpool Bay	53.4833	3.2500
J	Ramsay	54.3167	4.3667
K	Workington	54.6500	3.5667
L	Wylfa Head	53.4167	4.4667
M	Liverpool (GD)	53.4494	3.0167
N	Llandudno	53.3315	3.8237
O	New Brighton	53.4500	3.0333
P	Amlwch	53.4167	4.3333
Q	Ostg	53.5000	3.2167
R	Queens Channel	53.5167	3.2000
S	STD Irish Sea	53.7667	4.1167
T	STN10	53.7667	3.7167
U	STN34	54.1500	3.6667
V	STN35	54.6500	3.9167
W	Creetown	54.8667	4.4000
X	Conwy	53.2833	3.8333
Y	Barrow RI	54.0833	3.1667
Z	Barrow HP	54.0667	3.1667
AA	Barrow HS	54.0167	3.1833
BB	Morecambe	54.0833	2.8833
CC	Fleetwood	53.9236	3.0056
Offshore Gauges External To Eastern Irish Sea:			
	G	53.4333	5.3667
	33J	52.0667	5.7833
	B78	51.7500	6.6000
	C78	51.3333	6.5000
	F78	50.5500	7.5333
	F80	50.5333	7.6167
	D78	50.5833	6.1667
	G78	49.6000	8.6167
	G80	49.6667	8.5333

2
3

1
2
3

Table 2a: Latitude and longitude of current meters used in comparison tables

Point	Latitude (N)	Longitude(W)
2	54.6208	4.4750
3	54.5792	4.3583
6	54.5375	4.3417
8	54.5042	4.4083
9	54.4042	3.5583
12	54.2375	4.1917
15	54.2208	3.8750
16	54.1042	3.5583
18	54.0375	2.9417
23	54.0208	3.3417
24	54.0208	2.9917
32	54.0042	2.9583
33	53.9042	4.4083
34	53.8875	3.5083
35	53.8708	3.5250
38	53.7708	3.9250
44	53.7542	4.1250
50	53.6542	4.3750
56	53.5875	4.0917
57	53.5375	3.5583
58	53.4875	3.3083
59	53.4708	3.4917
60	53.4042	3.9417
61	53.3875	3.7583

4
5
6

Table 2b: Comparison of observed amplitude (h_o) (cms) and phase (g_o) (deg) and computed h_c , g_c from Calc 1, at offshore gauges

Gauge	M_2				M_4			
	Obs		Calc		Obs		Calc	
	h_o	g_o	h_c	g_c	h_o	g_o	h_c	g_c
STN 10	262	318	287	306	16.0	199	13.5	145
34	263	324	284	312	11.0	217	13.8	151
35	255	332	276	319	11.0	248	11.9	162
G	138	309	156	295	7.2	54	5.8	350
33J	111	183	97	180	3.8	19	5.6	287
B78	143	154	128	148	2.5	210	1.7	141
C78	164	151	152	149	3.5	223	3.2	138
F78	156	136	156	132	5.2	219	3.2	116
F80	151	136	153	132	4.4	218	3.1	116
D78	189	142	183	139	5.5	220	4.6	122
G78	138	121	142	120	2.9	231	0.9	105
G80	136	123	144	121	2.9	232	1.1	103

7
8

1 Table 3a: Comparison of observed amplitude (cm) and phase (degrees) (h_o , g_o) and
 2 computed (h_c , g_c) in the eastern Irish Sea (JD96) for the M_2 tidal elevation
 3

Point	Port	Observed		Calc 1		Calc 2	
		h_o	g_o	h_c	g_c	h_c	g_c
				G3AX		G3A	
A	Barrow	308	331	327	327	152	327
B	Birkenhead	311	323	323	312	301	310
C	Douglas	230	326	246	313	237	313
D	Heysham	315	325	329	316	319	314
E	Hilbre	292	317	321	308	313	305
F	Liverpool	312	323	322	313	296	312
G	Formby	312	315	316	307	305	305
H	Hestan	275	339	287	321	277	321
I	Liverpool Bay	262	315	321	305	302	305
J	Ramsay	262	328	261	315	251	314
K	Workington	273	332	293	318	280	317
L	Wylfa Head	206	300	235	290	221	290
M	Liverpool (GD)	307	321	323	311	303	309
N	Llandudno	267	308	293	300	280	299
O	New Brighton	306	318	323	311	307	309
P	Amlwch	235	305	256	294	244	294
Q	Ostg	290	315	322	306	304	304
R	Queens Channel	296	316	322	306	303	305
S	STD Irish Sea	235	317	263	305	246	304
T	STN10	262	318	290	306	275	305
U	STN34	263	324	287	312	271	311
V	STN35	255	332	279	318	266	317
W	Creetown	233	342	265	326	257	331
X	Conwy	241	318	224	299	136	299
Y	Barrow RI	306	329	163	321	312	319
Z	Barrow HP	292	327	324	321	312	319
AA	Barrow HS	297	325	317	315	300	311
BB	Morecambe	308	326	298	325	267	322
CC	Fleetwood	305	326	202	323	316	315

4
5

1 Table 3b: Comparison of observed amplitude (cm) and phase (degrees) (h_o , g_o) and
 2 computed (h_c , g_c) in the eastern Irish Sea (JD96) for the M_4 tidal elevation
 3

Point	Port	Observed		Calc 1		Calc 2	
		h_o	g_o	G3AX		G3A	
				h_c	g_c	h_c	g_c
A	Barrow	19	252	38	203	61	283
B	Birkenhead	23	217	27	150	56	252
C	Douglas	6	233	7	170	49	262
D	Heysham	20	243	9	216	68	269
E	Hilbre	20	203	28	160	17	128
F	Liverpool	23	214	30	150	53	254
G	Formby	25	235	18	158	58	250
H	Hestan	12	280	12	167	11	152
I	Liverpool Bay	21	196	20	142	17	132
J	Ramsay	7	237	10	154	51	263
K	Workington	13	253	13	166	58	270
L	Wylfa Head	4	182	2	195	47	218
M	Liverpool (GD)	22	202	33	152	56	248
N	Llandudno	12	181	13	130	56	233
O	New Brighton	23	198	32	154	27	142
P	Amlwch	6	185	6	143	50	225
Q	Ostg	17	196	22	144	16	133
R	Queens Channel	17	197	22	147	18	136
S	STD Irish Sea	6	201	8	142	7	132
T	STN10	16	199	13	143	12	132
U	STN34	11	217	13	149	12	136
V	STN35	11	248	11	160	11	140
W	Creetown	30	274	27	206	30	208
X	Conwy	26	216	40	223	54	231
Y	Barrow RI	30	274	70	281	62	274
z	Barrow HP	26	216	28	195	14	152
AA	Barrow HS	16	200	16	176	12	147
BB	Morecambe	11	217	33	246	34	239
CC	Fleetwood	11	248	68	254	62	249

4
 5
 6

1 Table 3c: Comparison of observed amplitude (cm) and phase (degrees) (h_o , g_o) and
 2 computed (h_c , g_c) in the eastern Irish Sea (JD96) for the M_6 tidal elevation
 3

Point	Port	Observed		Calc 1		Calc 2	
		h_o	g_o	h_c	g_c	h_c	g_c
				G3AX		G3A	
A	Barrow	3	49	14	35	14	176
B	Birkenhead	5	321	16	323	9	43
C	Douglas	1	354	1	67	1	55
D	Heysham	2	11	5	315	2	25
E	Hilbre	2	33	7	332	6	339
F	Liverpool	5	322	15	325	11	53
G	Formby	5	11	7	359	8	98
H	Hestan	-	-	1	72	3	250
I	Liverpool Bay	-	-	6	311	6	341
J	Ramsay	-	-	1	101	3	100
K	Workington	2	325	1	126	4	148
L	Wylfa Head	-	-	0	178	2	152
M	Liverpool (GD)	5	349	14	324	9	50
N	Llandudno	2	356	3	289	4	30
O	New Brighton	5	329	14	324	11	339
P	Amlwch	-	-	1	271	2	52
Q	Ostg	4	14	6	318	6	337
R	Queens Channel	3	18	7	321	7	347
S	STD Irish Sea	1	354	1	296	2	322
T	STN10	3	335	3	306	4	328
U	STN34	1	7	2	315	2	305
V	STN35	1	234	1	93	2	235
W	Creetown	5	117	13	65	4	123
X	Conwy	6	22	22	8	11	68
Y	Barrow RI	5	117	6	164	1	13
Z	Barrow HP	6	22	14	0	11	327
AA	Barrow HS	3	355	6	315	6	318
BB	Morecambe	1	7	16	15	16	5
CC	Fleetwood	1	234	8	108	9	323

4
 5
 6

1 Table 4a: Spatial variability of computed M₂ tidal elevation h_c(m) and phase g_c (degrees)
 2 with distance Δ(km) between nearest nodal points and observational point
 3

Port	Obs		Calc 1 (G3AX)				Calc 2 (G3A)			
	h _o	g _o	Δ	h _c	g _c	h(m)	Δ	h _c	g _c	h(m)
Hilbre	293	317	1.1	321	309	9.6	0.6	313	305	3.8
			1.1	275	307	2.0	1.0	304	306	17.4
			1.3	330	306	16.2	1.2	132	308	0.0
			1.8	296	307	2.3	1.5	305	304	8.6
Barrow RI	306	329	1.0	164	321	0.0	0.9	155	317	0.0
			1.0	161	312	0.0	1.6	312	319	9.9
			1.9	324	321	9.1	2.0	312	317	8.1
			2.2	327	326	6.4	2.2	198	318	0.7
Barrow HP	292	327	1.0	324	321	9.0	0.5	312	319	9.9
			1.1	323	322	6.0	1.6	312	317	8.1
			1.6	326	326	3.0	1.6	153	321	0.0
			2.0	164	321	0.0	2.6	198	318	0.7
Barrow HS	297	325	0.6	317	315	6.2	0.8	300	311	7.1
			1.9	325	315	5.4	1.6	306	312	5.5
			2.1	319	311	8.0	1.7	302	312	4.2
Morecambe	308	326	0.6	298	325	3.0	1.3	267	322	2.8
			1.5	322	323	3.7	1.5	158	319	0.0
			2.0	271	329	2.9	1.6	327	318	4.0
			2.0	214	326	0.9	2.0	231	329	1.3
Fleetwood	305	326	0.3	202	323	0.9	0.2	158	302	0.0
			1.0	221	319	1.0	1.3	136	319	0.0
			1.0	260	311	1.5	1.8	316	315	8.2
			2.3	331	315	9.6	1.9	130	329	0.0

4
5

1 Table 4b: Spatial variability of computed M_4 tidal elevation h_c (m) and phase g_c (degrees)
 2 with distance Δ (km) between nearest nodal points and observational point
 3

Port	Obs		Calc 1 (G3AX)				Calc 2 (G3A)			
	h_o	g_o	Δ	h_c	g_c	$h(m)$	Δ	h_c	g_c	$h(m)$
Hilbre	20	203	1.1	28	160	9.6	0.6	17	129	3.8
			1.1	35	228	2.0	1.0	22	147	17.4
			1.3	26	146	16.2	1.2	66	238	0.0
			1.8	31	212	2.3	1.5	15	120	8.6
Barrow RI	30	274	1.0	70	281	0.0	1.0	62	274	0.0
			1.0	64	276	0.0	1.1	64	278	0.0
			1.9	28	195	9.1	1.6	14	152	9.9
			2.2	33	203	6.4	2.0	14	170	8.1
Barrow HP	26	216	1.0	28	195	9.1	0.5	14	152	9.9
			1.1	28	200	5.9	1.6	14	170	8.1
			1.6	27	205	3.3	1.6	62	282	0.0
			2.0	70	280	0.0	2.3	63	278	0.0
Barrow HS	16	200	0.6	16	176	6.2	0.8	12	147	7.1
			1.9	15	173	5.4	1.6	9	148	5.5
			2.1	14	158	8.0	1.7	12	164	4.2
Morecambe	11	217	0.6	33	246	3.0	1.3	34	239	2.8
			1.5	19	181	3.7	1.5	60	286	0.0
			2.0	30	249	2.9	1.6	8	142	4.0
			2.0	55	286	0.9	2.0	46	272	1.3
Fleetwood	11	248	0.3	68	254	0.9	0.2	63	249	0.0
			1.0	63	256	1.0	0.5	56	273	0.0
			1.0	48	262	1.5	0.7	66	265	0.0
			2.3	13	162	9.6	1.8	5	140	8.2

4
5

1 Table 4c Spatial variability of computed M_6 tidal elevation h_c (m) and phase g_c (degrees)
 2 with distance Δ (km) between nearest nodal points and observational point
 3

Port	Obs		Calc 1 (G3AX)				Calc 2 (G3A)			
	h_o	g_o	Δ	h_c	g_c	h (m)	Δ	h_c	g_c	h (m)
Hilbre	2	33	1.1	7	332	9.6	0.6	6	339	3.8
			1.1	24	30	2.0	1.0	9	347	17.4
			1.3	7	303	16.2	1.2	4	64	0.0
			1.8	24	25	2.3	1.5	4	309	8.6
Barrow RI	5	117	1.0	6	164	0.0	1.0	1	12	0.0
			1.0	8	264	0.0	1.1	2	206	0.0
			1.9	14	0	9.1	1.6	11	327	9.9
			2.2	11	19	6.4	2.0	13	324	8.1
Barrow HP	6	22	1.0	13	0	9.1	0.5	11	327	9.9
			1.1	13	350	5.9	1.6	13	324	8.1
			1.6	9	2	3.3	1.6	6	190	0.0
			2.0	6	164	0.0	2.3	2	206	0.0
Barrow HS	3	335	0.6	6	315	6.2	0.8	6	318	7.1
			2.0	10	321	5.4	1.6	7	314	5.5
			2.1	7	298	8.0	1.7	8	317	4.2
Morecambe	1	7	0.6	16	15	3.0	1.3	16	5	2.8
			1.5	14	280	3.7	1.5	8	289	0.0
			2.0	10	27	2.9	1.6	10	296	4.0
			2.0	9	105	0.9	2.0	8	111	1.3
Fleetwood	1	234	0.3	8	108	0.9	0.2	9	323	0.0
			1.0	12	82	1.0	0.5	17	172	0.0
			1.0	24	27	1.5	0.7	1	274	0.0
			2.3	6	291	9.6	1.8	5	307	8.2

4
5

1 Table 5a: Comparison of observed semi-major axis A_o (cm s^{-1}) and orientation T_o (degrees)
 2 of the M_2 current ellipse at locations in the eastern Irish Sea used in JD96
 3

Rig No.	Observed			Calc 1 G3AX			Calc 2 G3A		
	A_o	T_o	h_o	A_c	T_c	h_c	A_c	T_c	h_c
2	110	9	33	106	3	42	107	6	47
3	97	7	48	109	11	51	96	11	51
6	86	171	53	92	5	49	83	5	49
12	32	46	30	42	25	25	41	46	28
15	37	38	25	44	25	26	40	30	24
16	35	168	25	40	179	26	34	172	25
23	49	148	20	67	165	18	49	157	20
33	79	18	60	89	20	58	88	58	58
44	75	5	46	86	5	45	80	5	45
50	89	7	57	101	7	54	101	8	56
56	79	175	46	84	176	46	87	176	47
60	58	169	28	63	169	25	56	168	24
61	48	166	20	54	163	19	54	160	15

4
 5 Table 5b: Comparison of observed semi-major axis A_o (cm s^{-1}) and orientation T_o (degrees)
 6 of the M_4 current ellipse at locations in the eastern Irish Sea used in JD96
 7

Rig No.	Observed			Calc 1 G3AX			Calc 2 G3A		
	A_o	T_o	h_o	A_c	T_c	h_c	A_c	T_c	h_c
3	5.0	34	48	7.0	7	51	5.2	7	51
6	4.3	20	53	5.7	4	49	3.7	6	49
12	10.7	42	30	4.3	28	25	3.8	45	28
18	21.9	64	3	25.3	56	6	23.9	65	8
23	4.8	7	20	2.6	59	18	2.0	44	20
24	9.8	52	7	18.6	62	10	19.6	10	10
32	11.9	54	11	15.5	55	9	15.4	59	9
33	6.3	29	60	6.4	20	58	5.7	20	58
44	5.8	11	46	6.3	9	45	5.2	11	45
50	7.0	19	57	6.6	8	54	5.9	6	55
56	6.0	10	46	7.1	5	45	6.2	5	47
57	5.1	165	33	5.6	167	30	4.2	158	29
58	3.4	172	16	6.8	172	13	4.6	160	12
59	4.5	180	20	5.7	169	17	4.0	153	21
60	5.5	171	28	5.0	175	25	4.4	163	24
61	4.7	186	20	3.6	161	19	3.8	131	15

8
 9
 10
 11
 12
 13
 14

1 Table 5c Comparison of observed semi-major axis A_o (cm s^{-1}) and orientation T_o (degrees)
 2 of the M_6 current ellipse at locations in the eastern Irish Sea used in JD96
 3

Rig No.	Observed			Calc 1 G3AX			Calc 2 G3A		
	A_o	T_o	h_o	A_c	T_c	h_c	A_c	T_c	h_c
2	3.1	2	33	2.9	179	42	3.0	177	46
8	2.5	110	40	3.3	160	41	3.5	0	42
9	0.7	146	19	1.9	164	19	2.5	134	17
15	1.0	139	25	1.9	145	26	1.9	134	24
23	1.0	159	20	6.7	160	18	3.3	136	20
24	2.3	64	7	8.7	41	10	12.0	108	10
32	1.9	3	11	5.5	60	8	7.2	39	9
33	1.3	4	60	1.8	6	58	2.3	3	60
34	2.5	161	25	3.3	4	24	3.3	178	25
35	1.6	6	25	4.2	179	17	3.2	159	21
38	1.5	173	42	2.6	177	42	2.6	169	42
44	1.2	167	46	2.6	0	45	2.8	178	45
50	1.6	184	57	2.7	3	54	3.0	179	55
56	1.4	163	46	2.8	173	46	3.2	176	46
57	1.8	162	33	2.9	170	30	2.9	160	29
58	2.1	153	16	4.1	149	13	3.1	170	12
59	1.6	185	20	4.2	179	17	3.2	159	21
60	2.0	165	28	2.8	168	25	2.4	167	24
61	1.0	174	20	2.3	158	19	2.6	157	15

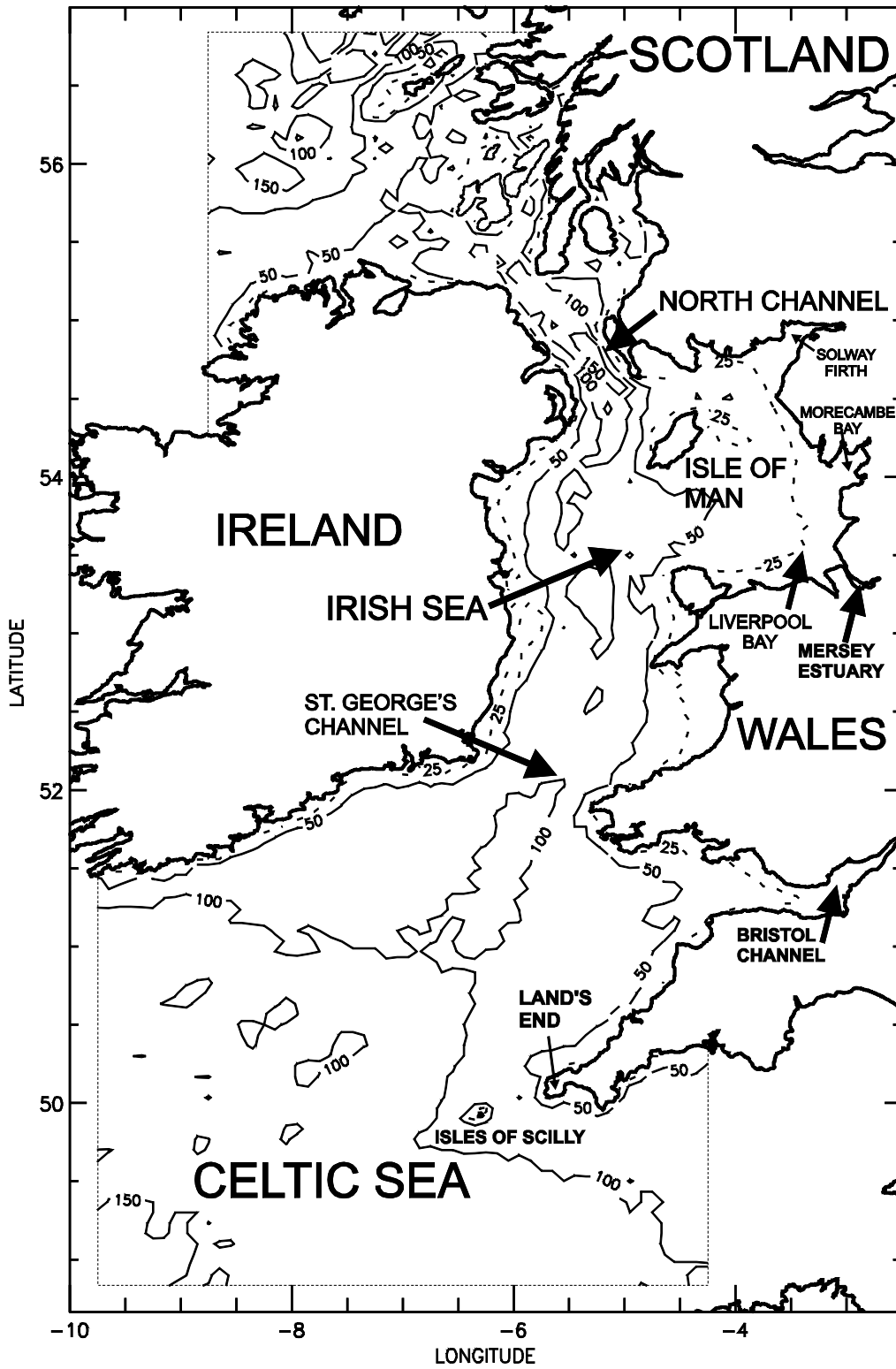
4
5

1 Table 6: Spatial variability of computed M_2 , M_4 and M_6 tidal ellipse semi-major axis A_c (cm
2 s^{-1}) and orientation T_c (degrees) with distance Δ (km) between nearest nodal points and
3 observation point
4

Rig No	Observed			Calc 1 G3AX				Calc 2 G3A			
	A_o	T_o	h_o	Δ	A_c	T_c	h_c	Δ	A_c	T_c	h_c
M_2 Tide											
15	37	38	25	2.2	44	24	26	0.6	40	30	24
				3.0	40	23	23	4.2	39	28	26
				4.0	30	7	32	4.5	30	25	28
16	36	168	25	1.0	40	180	26	1.4	34	172	25
				3.3	38	165	25	2.2	38	1	26
				3.7	37	158	25	2.2	39	177	25
23	49	148	20	0.9	68	165	18	0.7	49	157	20
				2.6	41	148	17	2.5	52	154	15
M_4 Tide											
6	4.3	20	53	2.4	5.7	4	48	1.8	3.7	6	49
				3.7	5.9	7	53	1.8	5.3	6	48
				4.8	6.7	6	47	2.0	4.3	1	50
				4.8	5.3	19	50	3.2	5.3	16	47
18	21.9	64	3	0.3	25.2	56	6	0.8	24.0	65	8
				1.5	23.3	100	3	1.4	29.9	72	0
				1.6	11.8	100	8	1.8	22.2	68	0
				1.9	28.6	63	3	1.9	35.1	58	11
M_6 Tide											
23	1.1	159	20	0.9	55.5	157	18	0.7	3.3	136	20
				2.6	3.0	152	17	2.5	5.2	152	15
				2.8	3.4	154	23	2.7	3.4	152	16
24	2.3	64	7	1.3	9.1	54	10	1.2	12.0	108	10
				1.5	3.6	59	11	1.4	6.7	54	10
				1.7	9.7	79	9	2.0	7.3	2	13
32	1.9	3	11	1.0	4.1	166	8	0.8	7.3	39	9
				1.6	3.5	59	11	1.5	8.0	54	10
				1.7	14.2	122	5	1.6	9.5	137	1

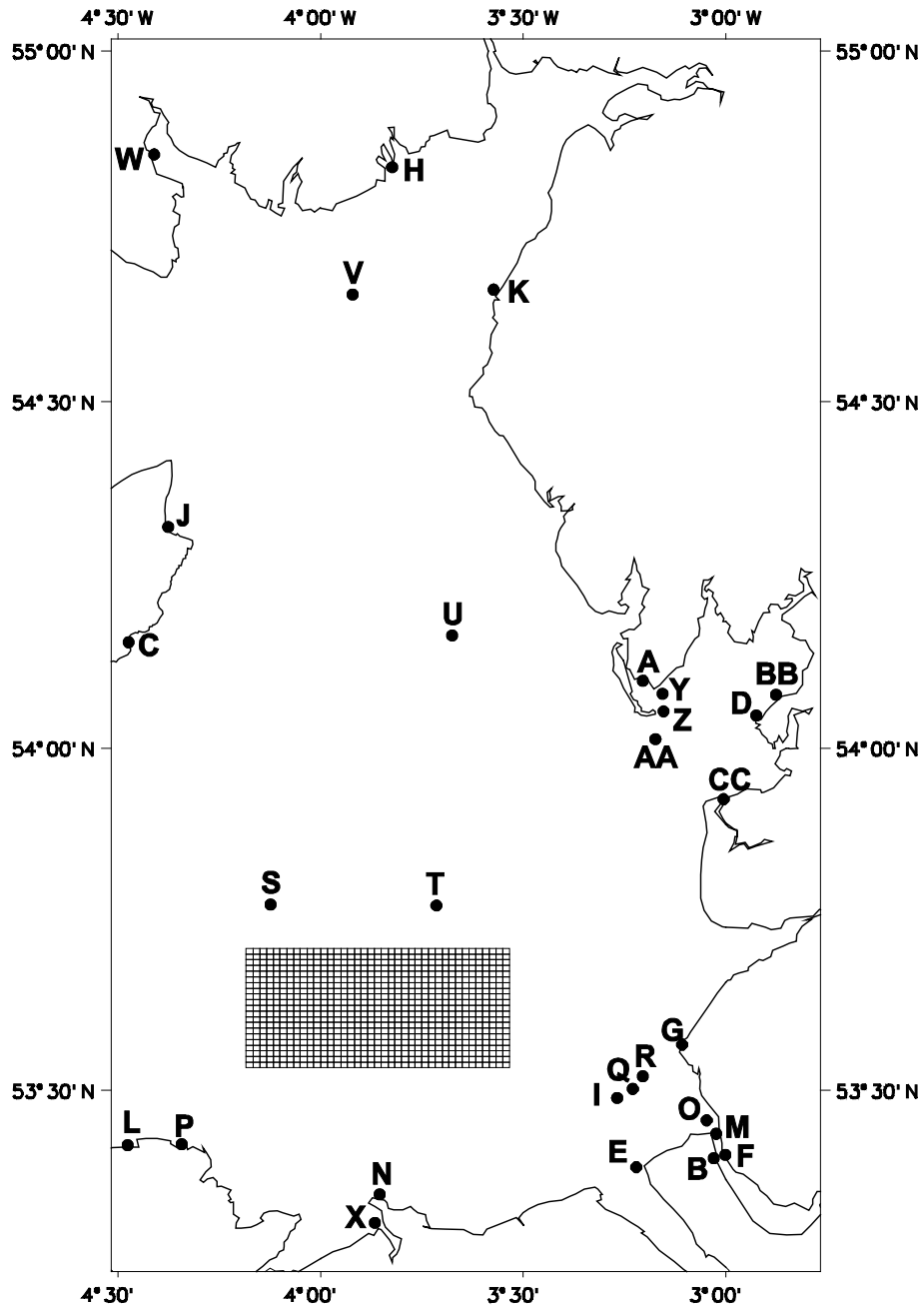
5
6
7
8

1 FIG1(a)



2

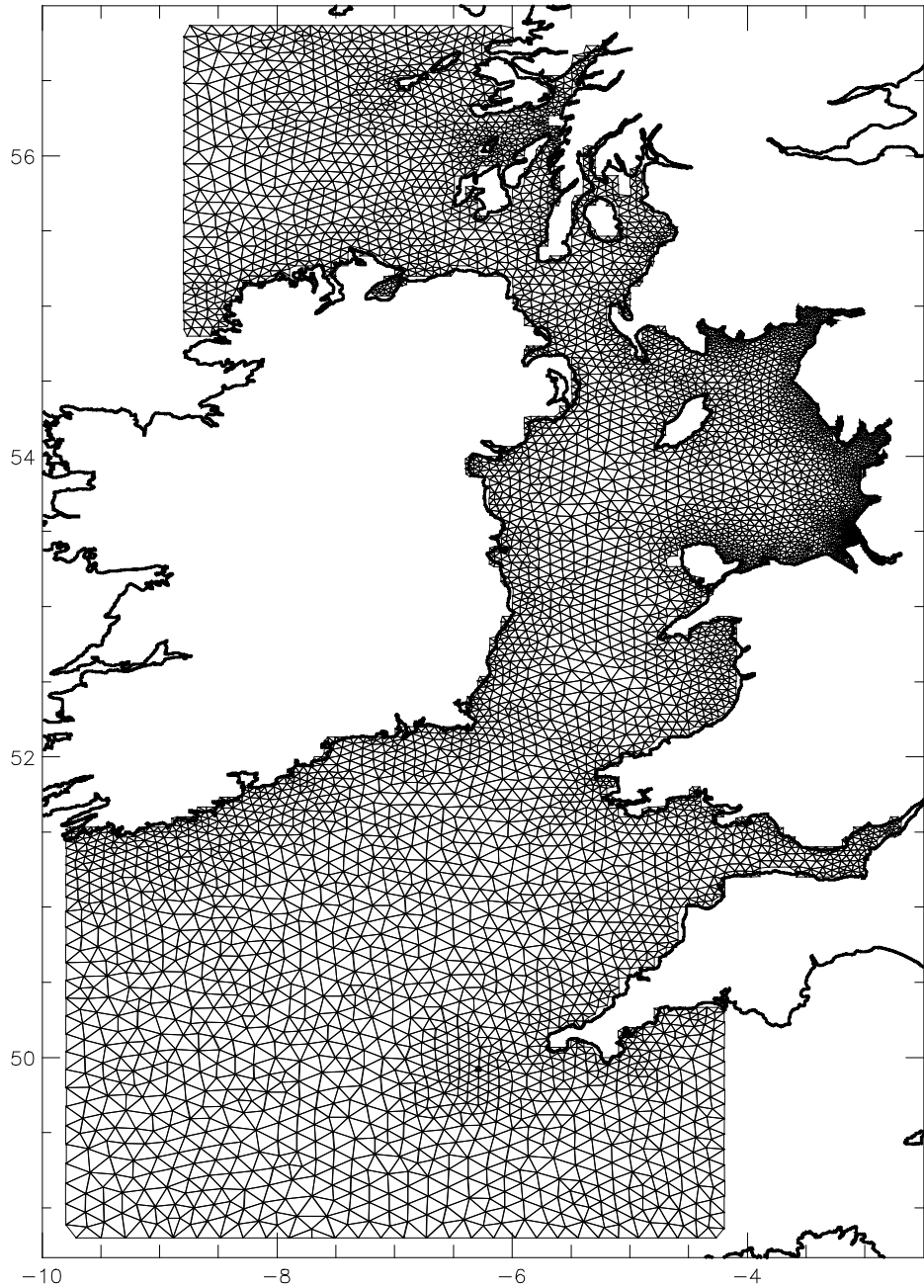
1 FIG2



- 2
- 3
- 4
- 5

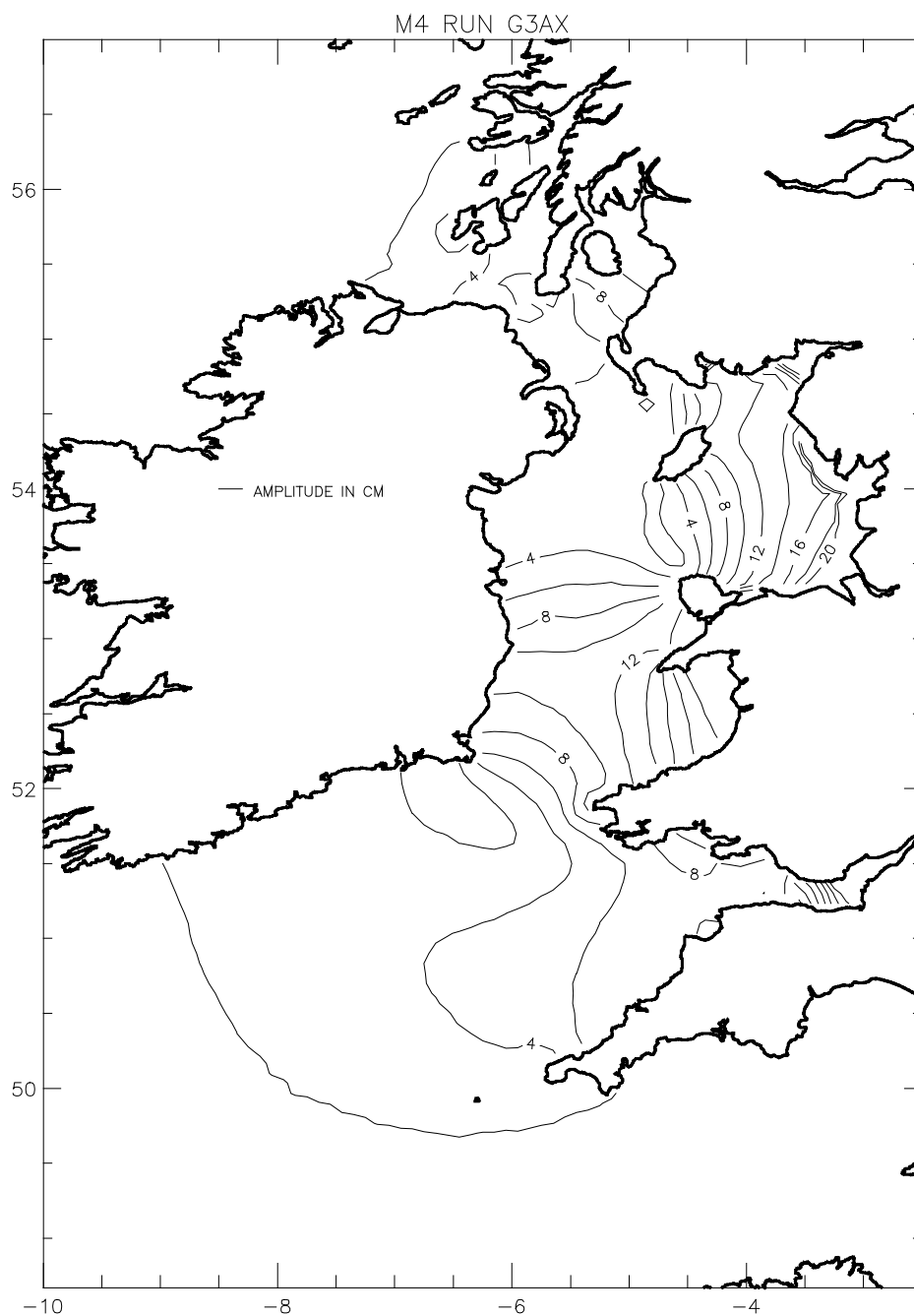
1 FIG3

GRID G3AX



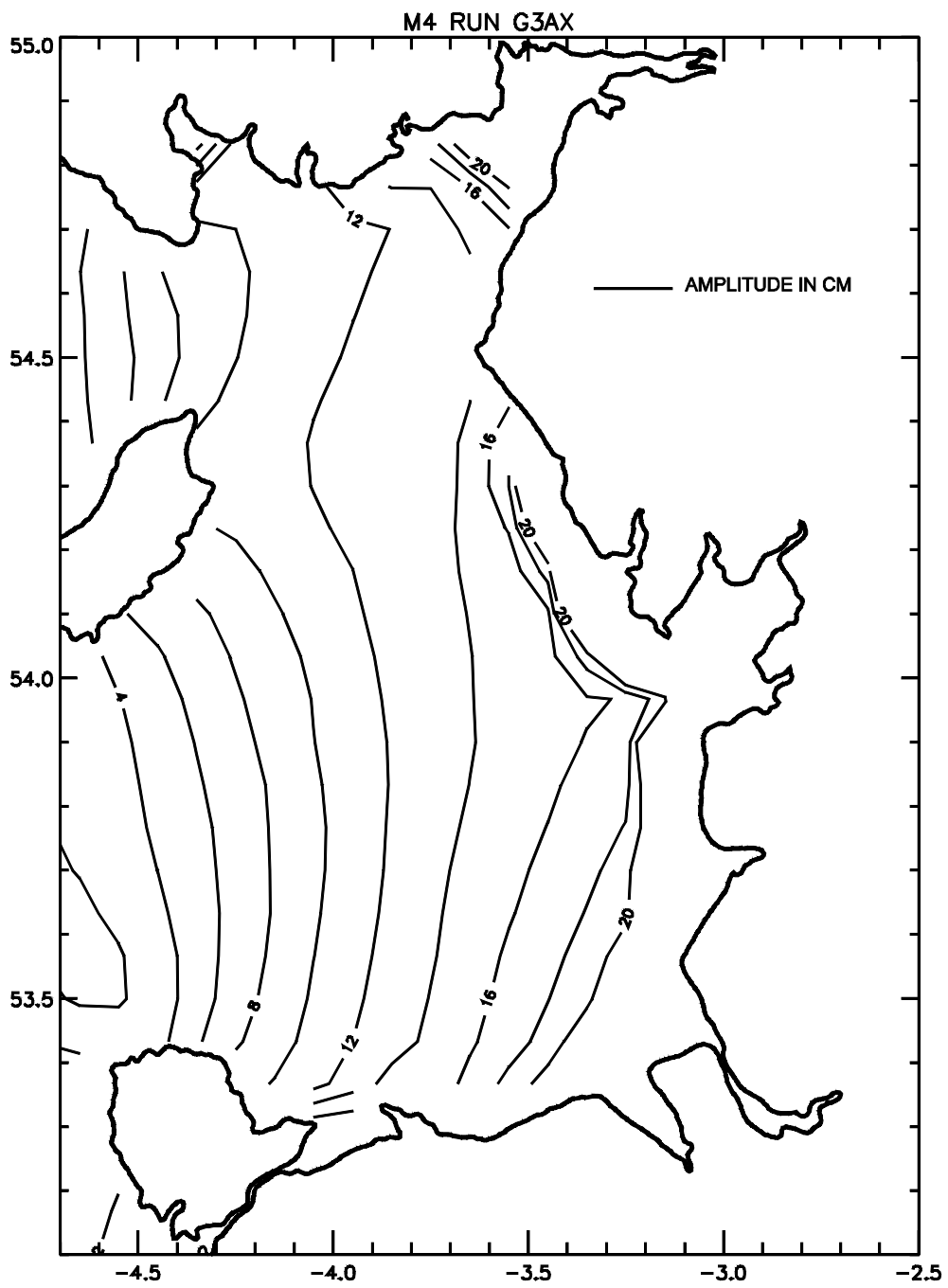
2
3
4

1 FIG4a(i)



2
3
4

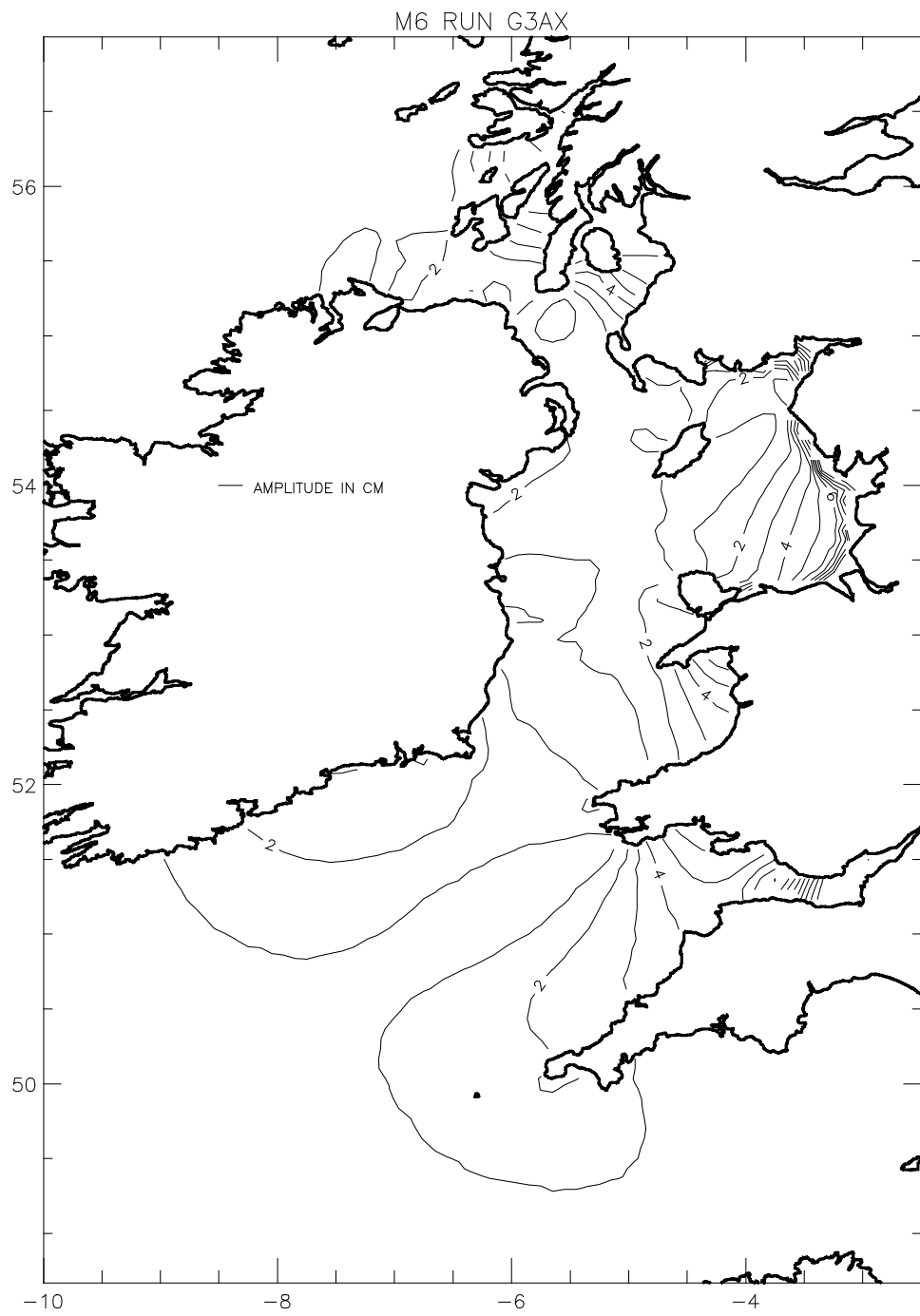
1 FIG4a(ii)



- 2
- 3
- 4

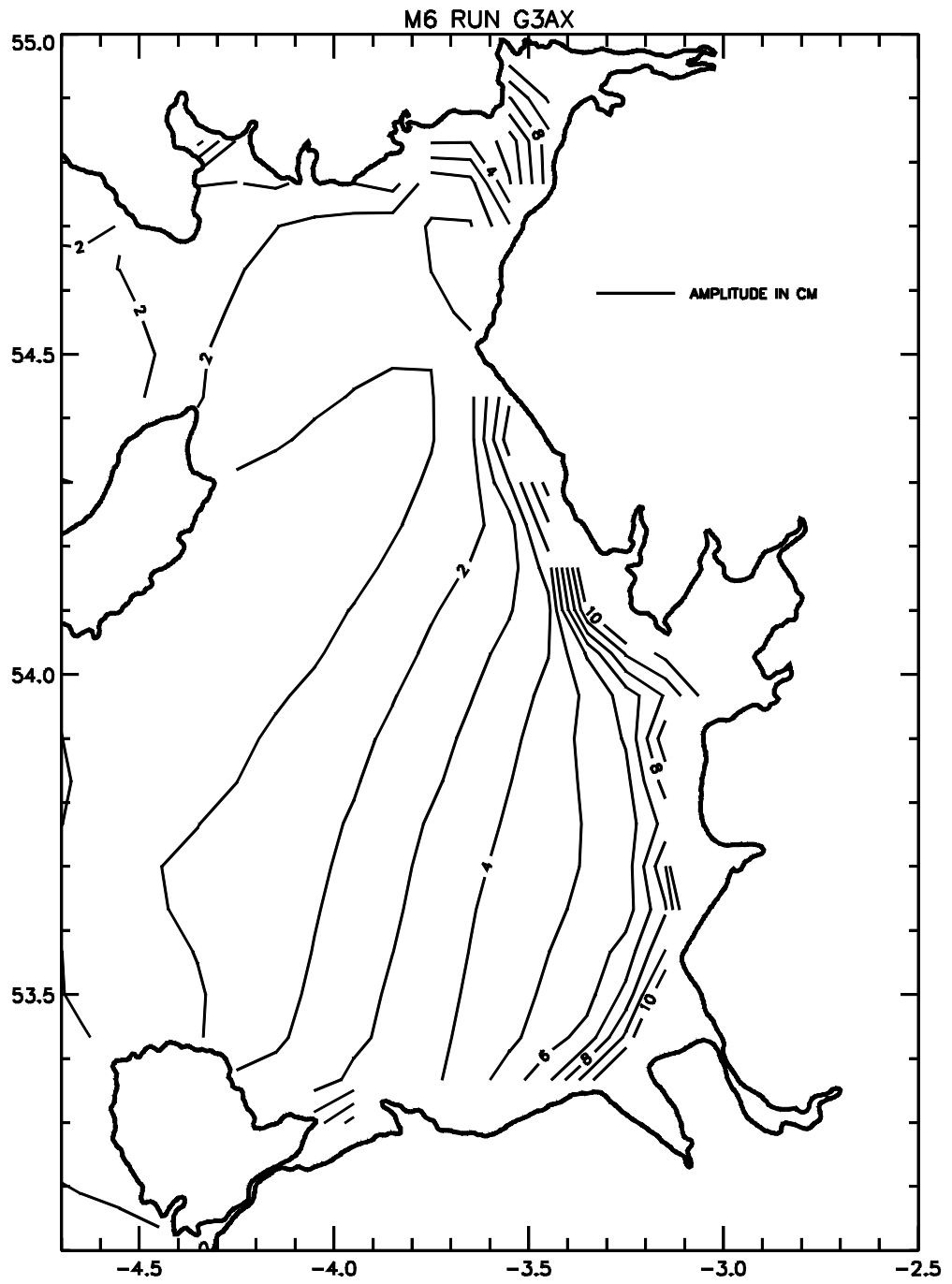
1 FIG4b(i)

2



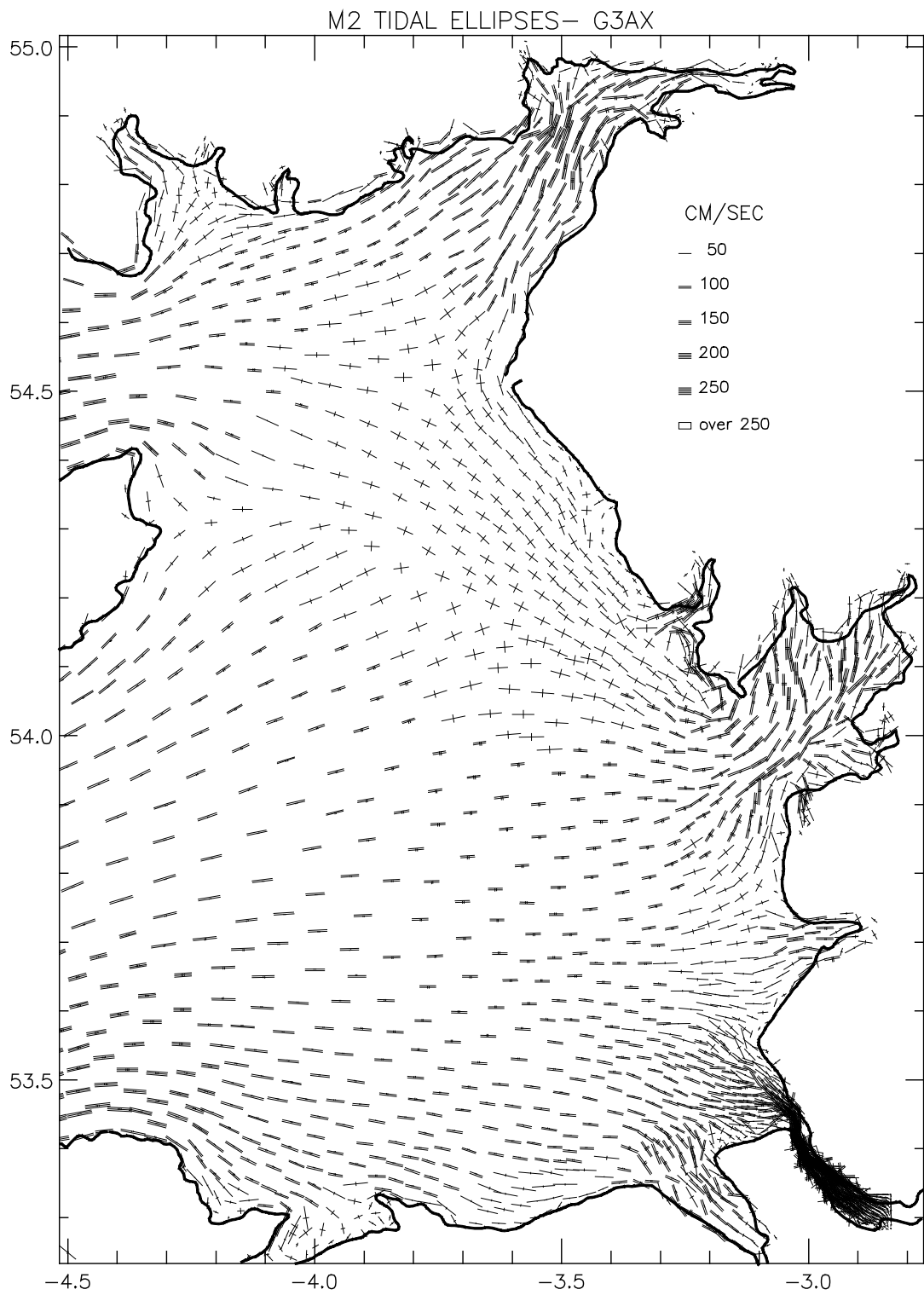
3

1 FIG4b(ii)



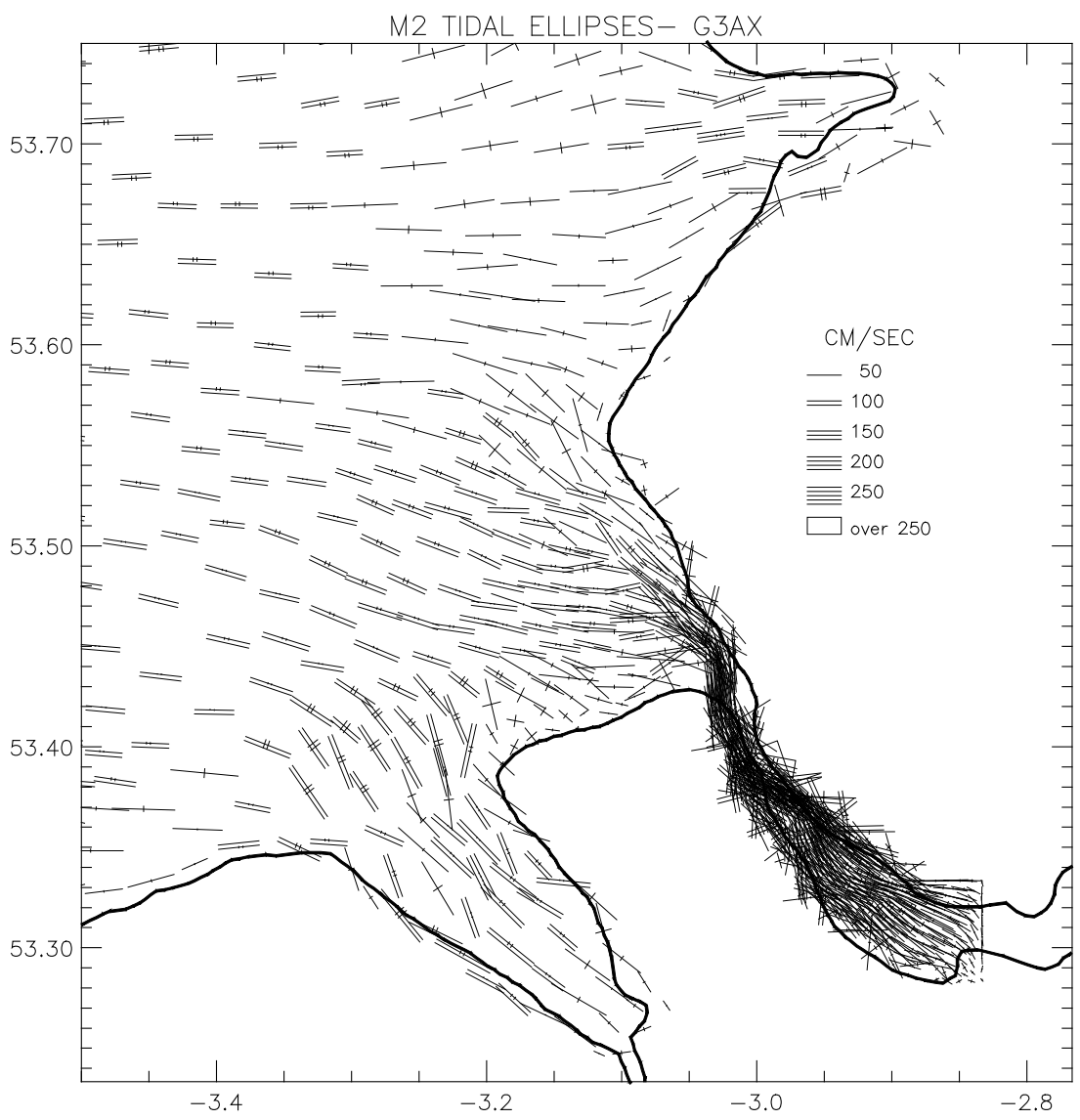
- 2
- 3
- 4

1 FIG5a(i)



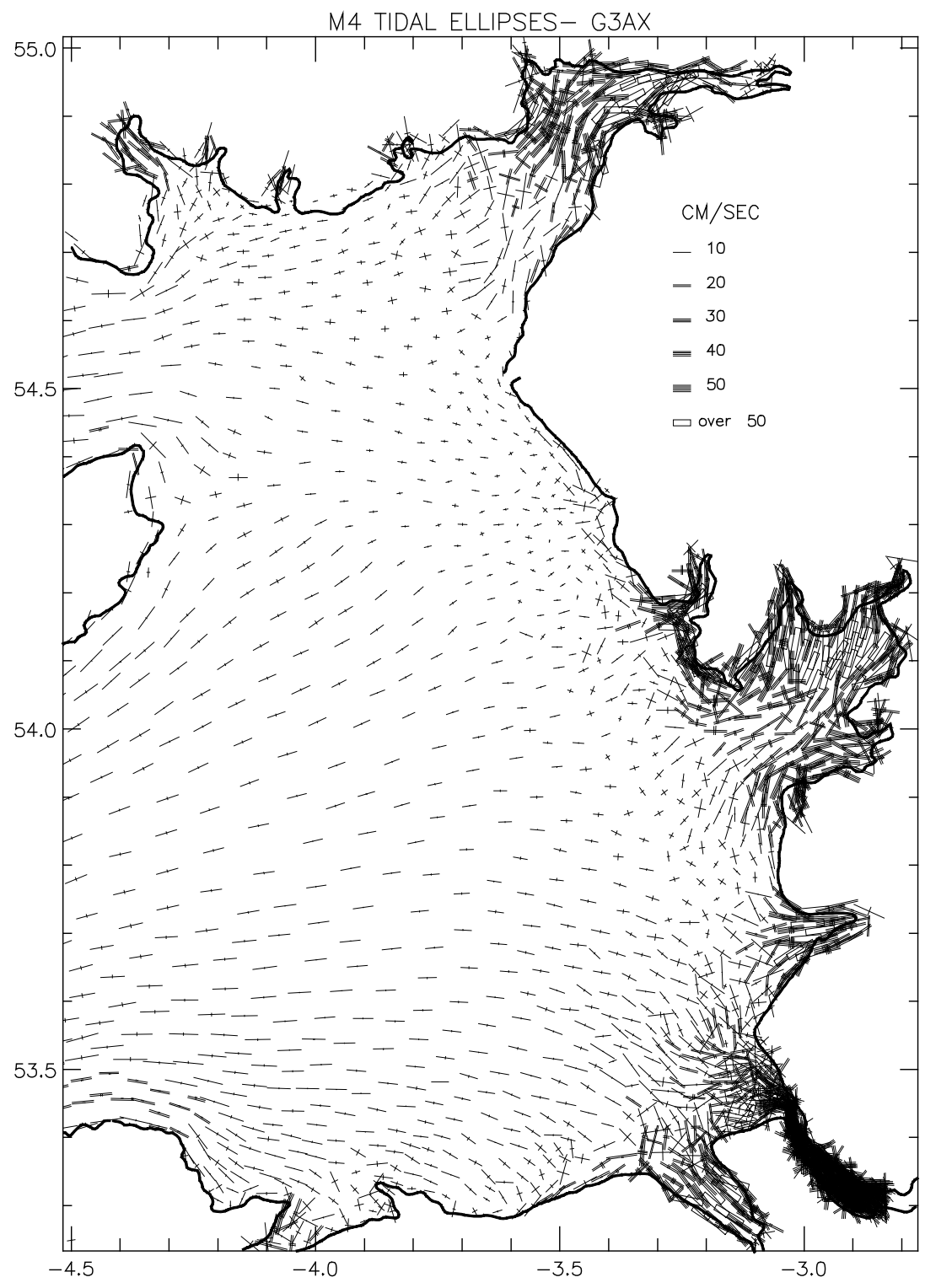
2
3
4
5
6

1 FIG5a(ii)



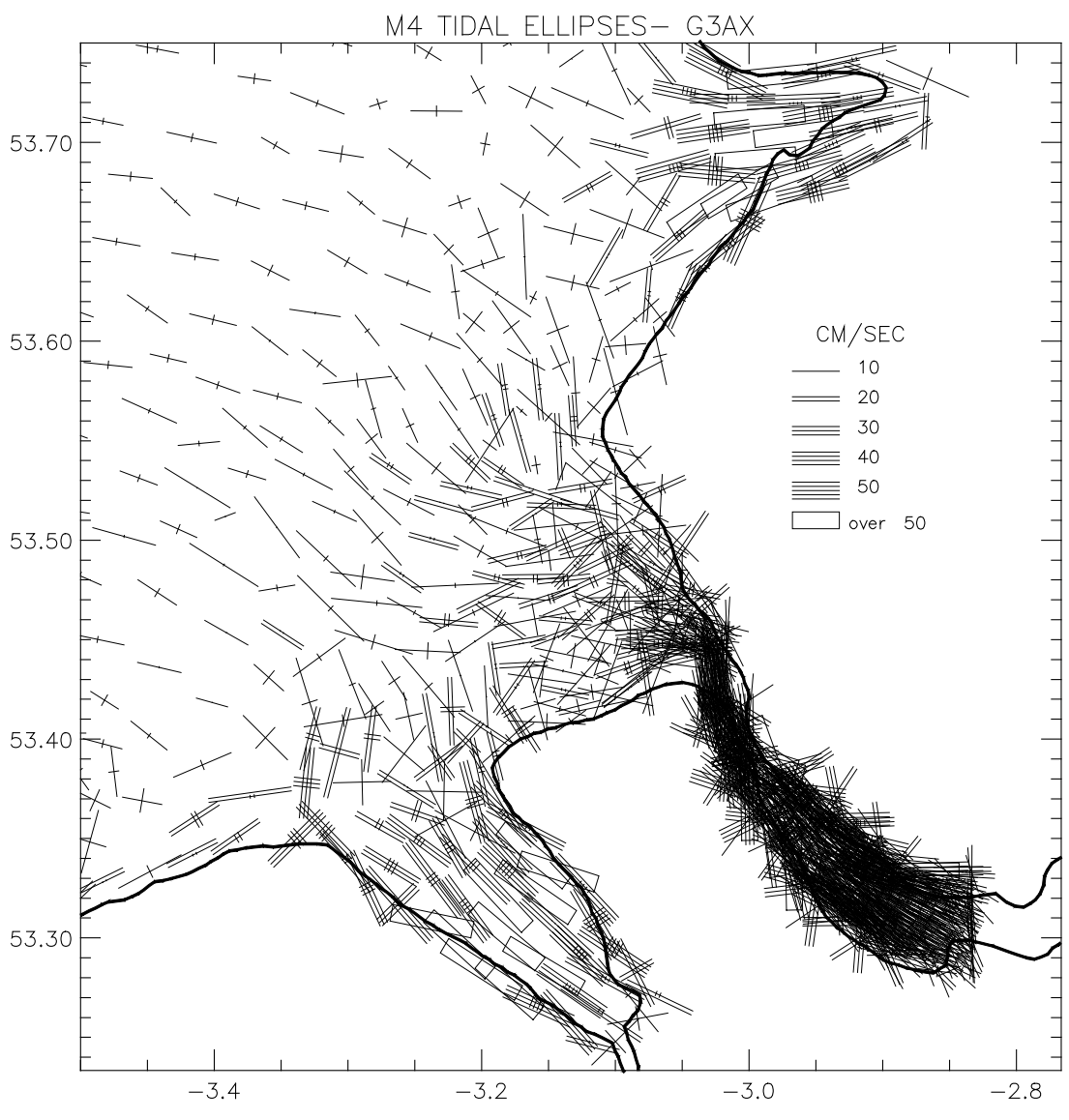
- 2
- 3
- 4
- 5
- 6
- 7
- 8
- 9
- 10
- 11
- 12
- 13

1 FIG5b(i)



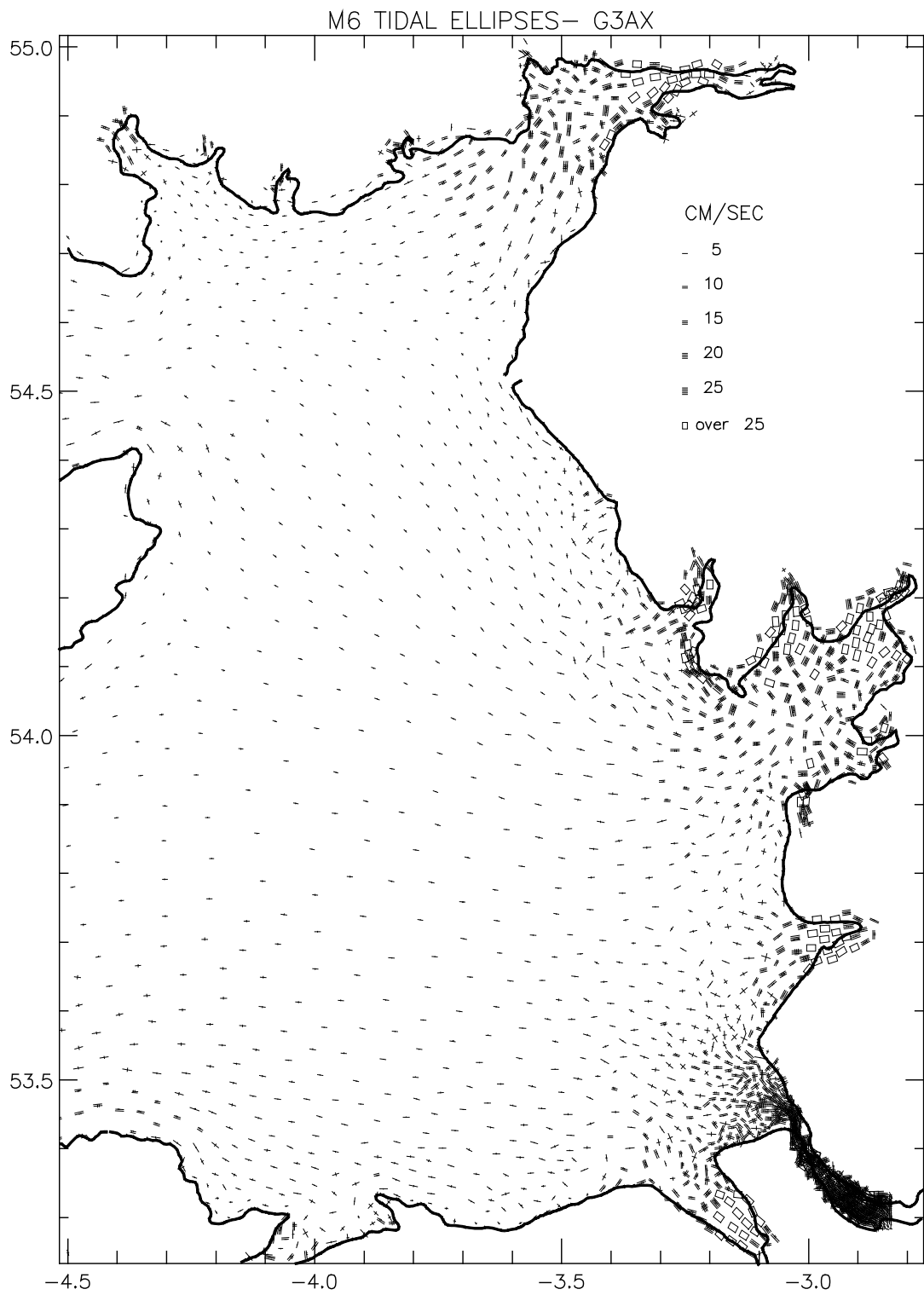
- 2
- 3
- 4
- 5
- 6

1 FIG5b(ii)



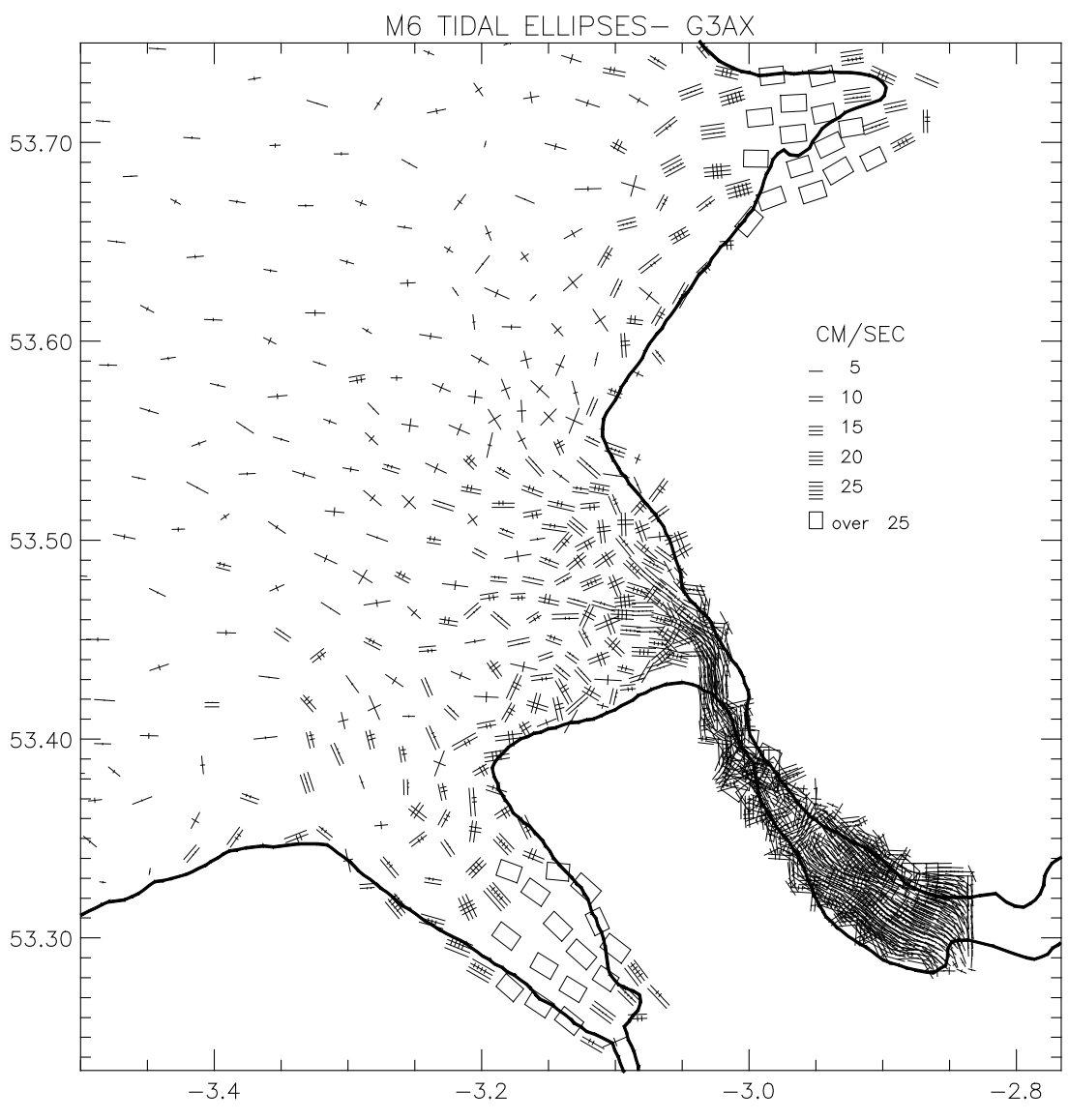
- 2
- 3
- 4
- 5
- 6
- 7
- 8
- 9
- 10
- 11
- 12
- 13

1 FIG5c(i)



2
3
4
5
6

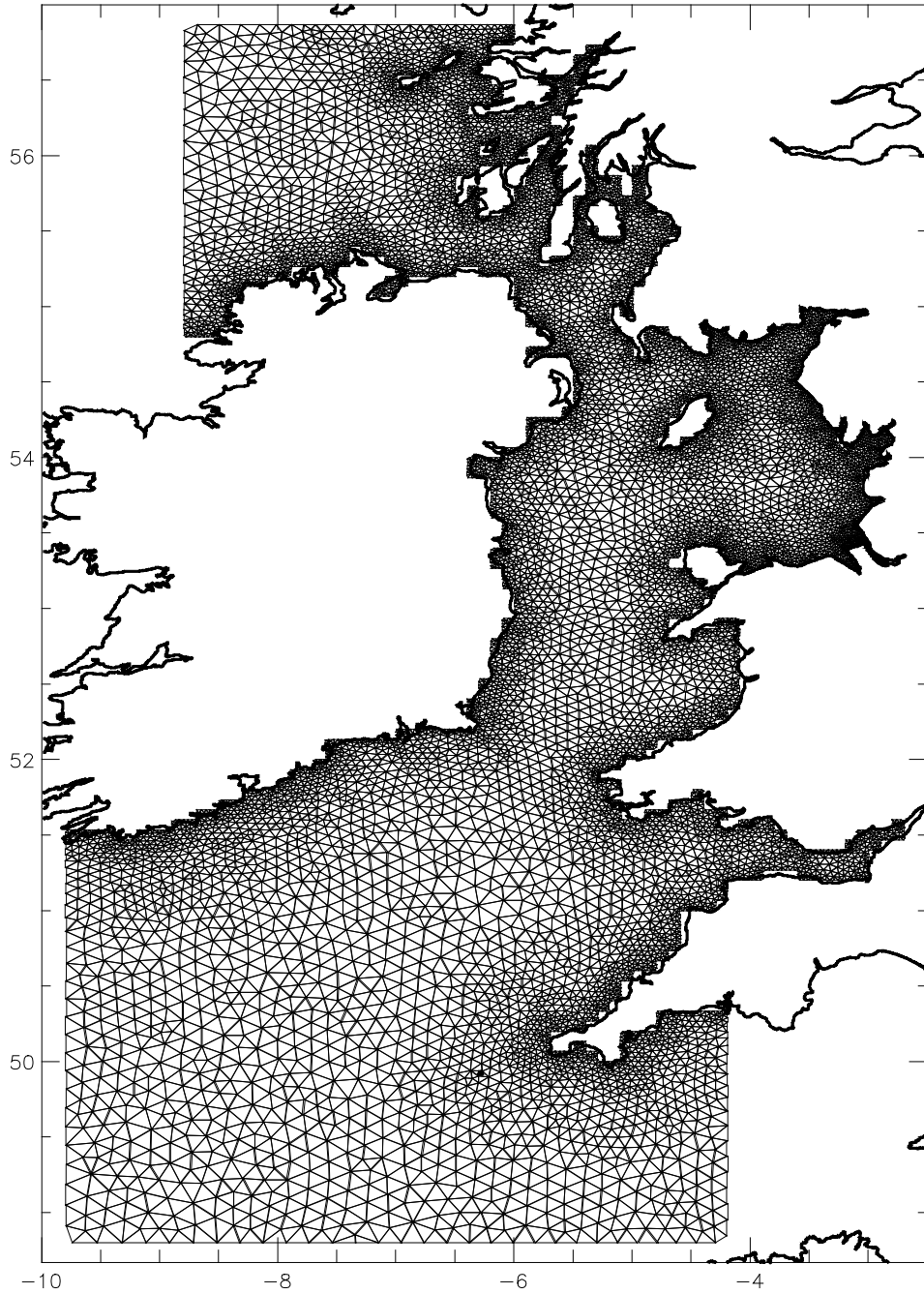
1 FIG5c(ii)



- 2
- 3
- 4
- 5
- 6
- 7
- 8
- 9
- 10
- 11
- 12
- 13

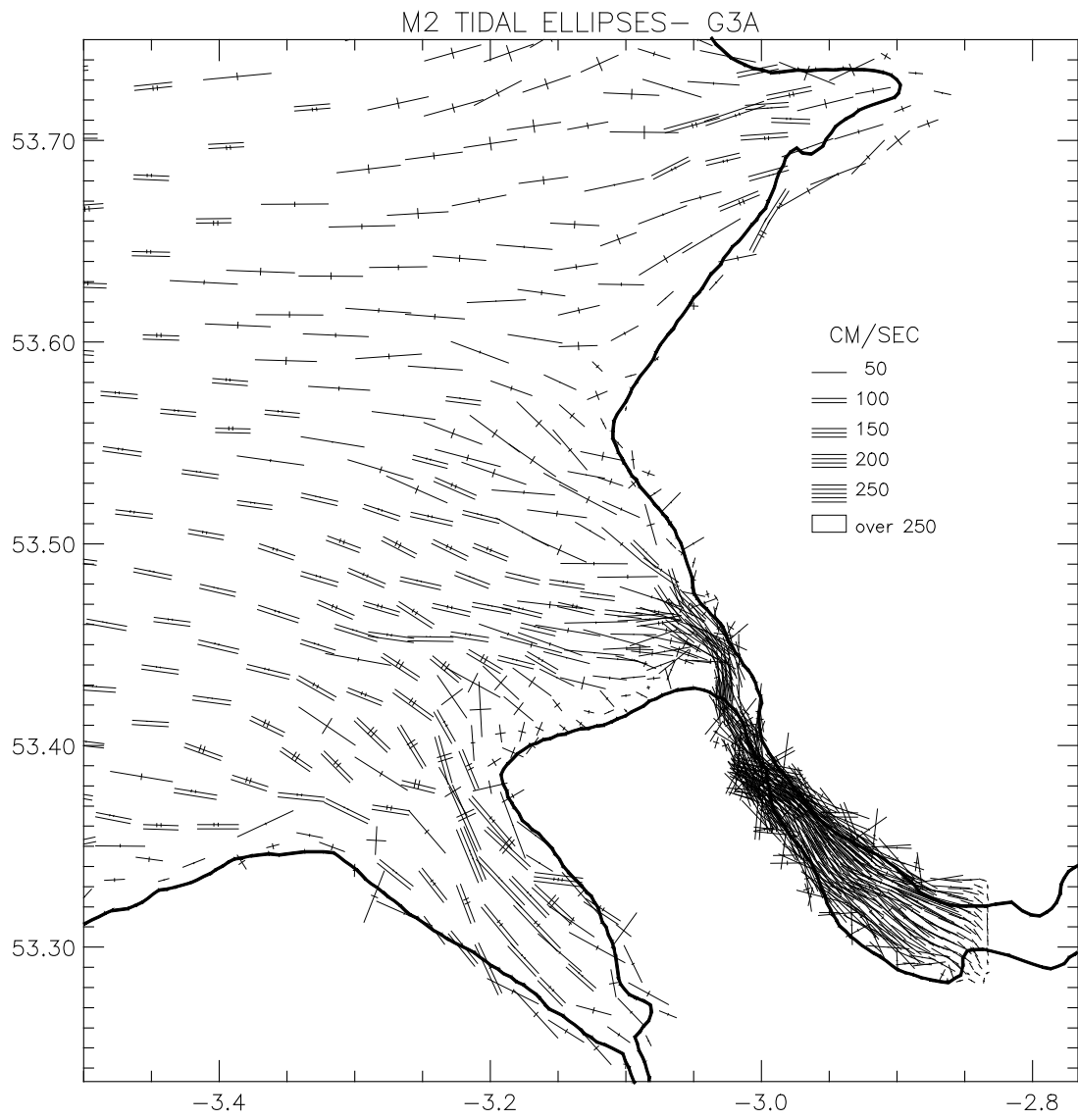
1 FIG 6

GRID G3A



2
3
4

1 FIG7a



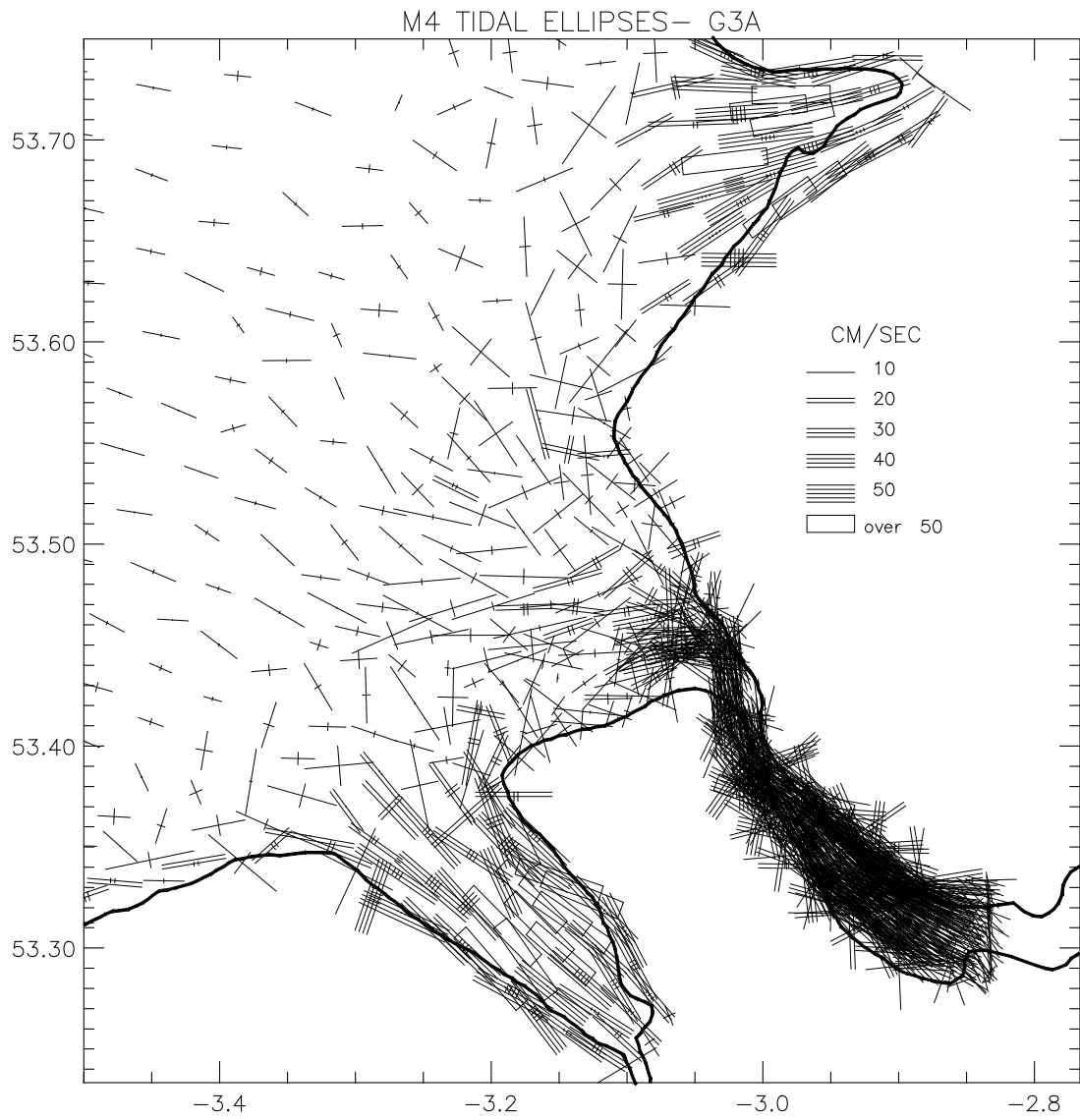
2

3

4

1 FIG 7b

2

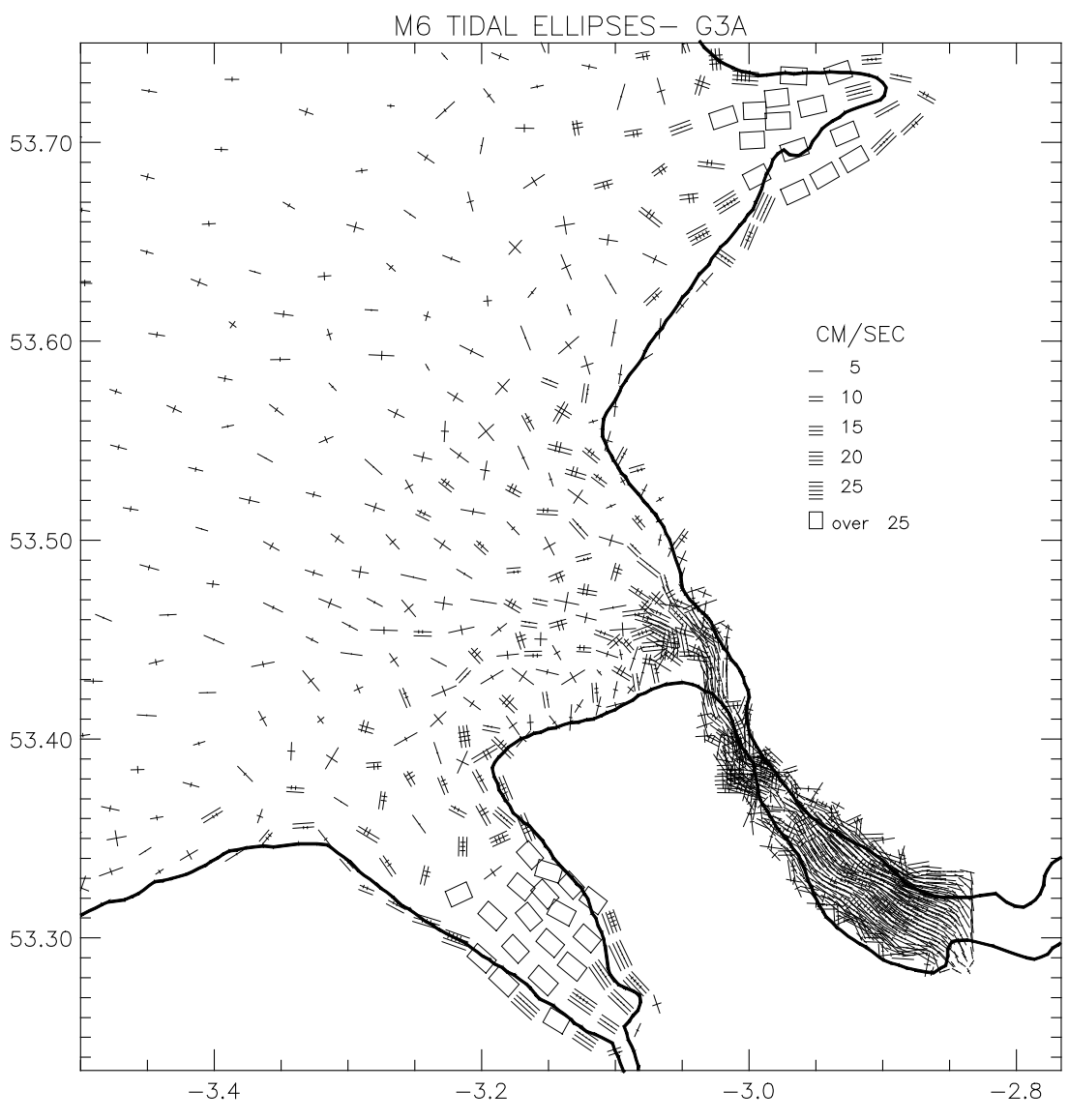


3

4

5

1 FIG 7c



2